Quantum Engineering Design

Short Term Course

Under the Japan-East Asia Network of Exchange for Students & Youths(JENESYS) program

Final Report

Quantum Engineering Design Course
Osaka University, Japan
September, 2010

A Density Functional Theory Study on Oxaliplatin Hydrolysis and Complex Formation with Guanine

Submitted as part of the fulfillment of the requirements for the QED-C Short Term Program

Eric M. Doña

Mutations in the genetic material of cells could cause uncontrollable cell division, effectively bypassing the cell cycle's natural control mechanisms. Such a condition is medically defined as a *malignant neoplasm* (more commonly known as cancer). Various types of cancer collectively account for more than seven million deaths worldwide on an annual basis (approximately 12-13% of total casualties per year). Three major conditions characterize cancer, namely:

- Division without regard for restrictive cell division limits
- Invasion of adjacent tissues and organs
- Spreading of the disease to distant parts of the body, called *metastasis* (usually in more advanced stages)

The term 'malignant' denotes the disease's rapidly progressing nature, as opposed to a *benign neoplasm*, which is simply formed by an abnormal growth of cells and lacks the three aforementioned criteria for malignancy.

Cancer is commonly brought about by effects of external cancer-causing agents (collectively given the term *carcinogen*) such as radiation or certain chemicals, or in some cases, from abnormalities present since birth (e.g. DNA replication errors). These effects give rise to genetic mutations which affect two types of genes found to be of particular importance with regards to the prevention, or alternatively, progression of cancer: *proto-oncogenes* and *tumor suppressors*.

Proto-oncogenes are responsible for promotion of cell division and inhibition of *apoptosis* (the process of programmed cell death). Mutations in proto-oncogenes turn them into the defective *oncogenes*, which then allows for rampant cell growth. In contrast, tumor suppressors perform the task of inhibiting cell division and promoting apoptosis. In this case, mutations take away the ability to initiate apoptosis, thus having the net effect of uninhibited cell proliferation. However, tumor suppressors are different from proto-oncogenes in that both *alleles* (an allele is one of a series, usually a pair, of alternative forms of a gene) should be damaged in order to produce ill effects. For proto-oncogenes, damage to one allele is enough to turn them into oncogenes, due to the mutant allele being dominant. Mutant tumor suppressor alleles, on the other hand, are recessive.

While research dealing with the genetic processes that ultimately result in cancer has considerably progressed, this new-found information has yet to be applied in developing novel and

effective cures for this class of diseases. In cases where the cancer is detected at an early stage, surgical procedures and/or radiation therapy are commonly used; however, in advanced stages, especially those wherein affected cells have metastasized to various parts of the body, chemotherapy plays a central role in combating the further spread of affected cells.

During a study involving the possible effect of electric current on cell division of *Escherichia coli*, it was found that cell division was inhibited not by the current itself, but by production of cisplatin [cis-diamminedichloroplatinum(II)] from the platinum electrodes.

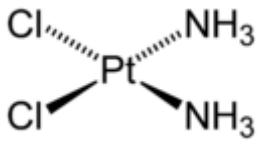

Fig. 1. Structure of cisplatin, the first clinically-approved platinum-based anti-cancer agent.

Cisplatin was then found to exhibit powerful anticancer activity; it achieves this by forming adducts with its major cellular target, DNA. Specifically, the platinum atom binds to the N7 atom of the purine bases guanine (G) and adenine (A), with guanine being preferred over adenine. To do this, the chlorine ligands act as leaving groups while the molecule undergoes aquation (i.e., replacing the Cl atoms with H_2O moieties). These H_2O groups themselves then function as leaving groups, and are replaced with the purine bases, creating one of the following possible DNA linkages: intrastrand d(GpG) (major product), intrastrand d(ApG), or interstrand cross-links.

In a proposed mechanism for cisplatin hydrolysis, the water ligand displaces chloride ion through a second-order nucleophilic substitution reaction (S_N2). The substitution reaction is believed to follow the sequence "reactant, first intermediate, transition state, second intermediate, and product." The first water molecule is believed to approach Pt along the equatorial plane in a 5-coordinate trigonal bipyramidal transition state where a chlorine atom, amine, and Pt lie, and then substitution of the remaining chlorine by a second water molecule follows. It was then found that reactions involving a transition state structure with smaller L-Pt-E angles and longer Pt-L and Pt-E bonds yield smaller activation energies (where L and E are the leaving and entering ligands, respectively).

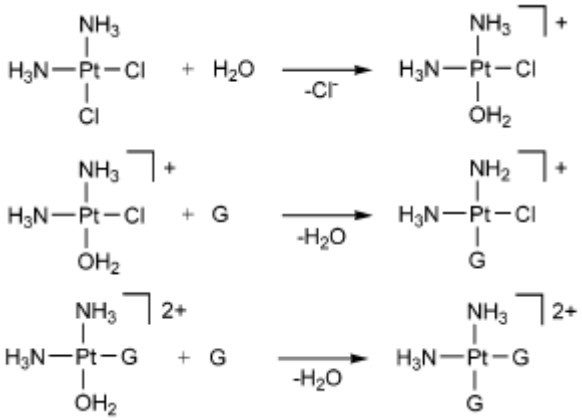

Fig. 2. Possible binding modes in the hydrolysis and DNA adduct formation of cisplatin. H_2O ligands replace Cl groups, after which they are in turn displaced by guanine molecules (signified by G).

Although cisplatin has proven to be effective in treating certain types of cancer (especially testicular cancer), several drawbacks still exist, one of which is the accumulation of various kinds of organ damage such as nephrotoxicity (kidney), ototoxicity (ear), and peripheral neuropathy (nervous system). Another hindrance is the limitation of cisplatin efficacy by cell lines which have (inherent or acquired) resistance to the drug. Development of novel Pt-based anticancer agents therefore becomes a crucial means of circumventing such limitations.

One such analogue currently approved for clinical administration is oxaliplatin [1,2-diaminocyclohexane (ethanedioate-O,O)platinum(II)]. It differs from its parent compound, cisplatin, due to the presence of oxalate (hereafter shortened to Ox) and diaminocyclohexane (denoted by the abbreviation DACH) functional groups. Oxaliplatin sparked interest when it, along with other DACH complexes, displayed antitumor activity against cisplatin-resistant tumor cells. In addition, oxaliplatin, like cisplatin before it, binds preferentially to guanine over adenine. It has also been suggested that nucleophiles such as endogenous HCO_3^- and $H_2PO_4^-$ displace the oxalate group in oxaliplatin, eventually leading to the formation of aqua complexes, which are being implicated for the cytotoxic effect of oxaliplatin through DNA adduct formation just like its parent molecule cisplatin. However, unlike cisplatin and its hydrolysis, no theoretical studies involving the hydrolysis of oxaliplatin have so far been conducted.

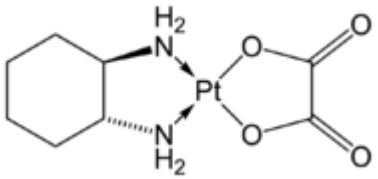

Fig. 3. Structure of oxaliplatin. Bears a similar structure to cisplatin (four-coordinated platinum, square planar), save for the DACH group on one side (left) and the oxalate group on the other (right).

It has been suggested that endogenous HCO_3^- and $H_2PO_4^-$ nucleophiles play an important role in displacing the Ox group in oxaliplatin, eventually leading to the formation of aqua complexes, which are being implicated for the cytotoxic effect of oxaliplatin through DNA adduct formation. A recently proposed mechanism for the first hydrolysis of oxaliplatin involves the formation of hydroxyl complexes (Pt-OH instead of Pt-H_2O) resulting from the deprotonation of the water molecule that binds to Pt after the initial ring-opening of the Ox group. However, the study was done under alkaline condition. It should be noted that hydroxide ion (OH^-) is a stronger nucleophile than water, and as such is more expected to readily act as one in a nucleophilic substitution reaction.

Another important issue surrounding oxaliplatin is its structure after binding with guanine bases of DNA. Previous studies show that the overall structure of the Pt-diguanine (Pt-G_2DACH) adducts measured by NMR is somewhat different from those in the solid-phase measured by X-ray diffraction. It is unclear whether the differences in the experimentally determined structures arise from the crystal packing constraints in the solid phase or the inability of NMR techniques to accurately measure the Pt-G_2DACH geometry in solution. A fact worthy of note is that the X-ray crystal structure of the cisplatin-G_2 complex has also been found to differ substantially from all NMR solution structures, even when the NMR and crystalline structures correspond to the same dodecamer sequence.

Unlike cisplatin, the hydrolysis and guanine-binding behavior of oxaliplatin has not yet been theoretically investigated. Thus, the present work aims to:

1) Examine the possible binding modes of water and hydroxide on oxaliplatin and propose an energetically feasible reaction path for hydrolysis, and
2) Examine the complexes formed by the binding of oxaliplatin to guanine and compare the results of our calculations with those obtained from NMR and X-ray diffraction studies.

Hence, it is imperative to shed light upon the differences in the results obtained by the different methods.

Density functional theory (DFT) calculations using the B3LYP exchange-correlation functional as incorporated in the Gaussian03 software package were employed to simulate all systems. First-row elements were treated using the 6-311+G(d,p) basis set, while the LanL2DZ with effective core potential (ECP) basis set was used for platinum. The geometry of oxaliplatin and its complexes with hydroxide, water and guanine were optimized in the singlet state. Transition state optimization was carried out using the Synchronous Transit-Guided Quasi-Newton (STQN) algorithm. For most systems, the Polarizable Continuum Model was used to correct for solvation effects.

The calculated bond lengths and bond angles for oxaliplatin (Table 1) accurately reproduce previously reported experimental values. We also considered the hydrolysis products of oxaliplatin and their hydroxyl (OH^-) counterparts. Our calculations (Table 2) show that the diaqua-

Pt complex (Fig. 5) is more stable than the corresponding aqua-hydroxy (Fig. 6) and dihydroxy-Pt (Fig. 7) complexes—products which were observed under strongly basic conditions—signifying that increasing the hydroxylation of Pt leads to a decrease in stability of the resulting complex in gas phase. However, it should be noted that solvent effects play an important role in deprotonation (the solvation energy of H^+ is around -11.7 eV). Therefore, the proposed mechanism involving hydroxyl complexes should not be ruled out.

Table 1. Calculated and experimental oxaliplatin bond lengths and bond angles.

Parameter	Calculated (w/o PCM corrections)	Calculated (w/ PCM corrections)	Experimental
Pt-O_1 bond distance, Å	2.00	2.06	2.01
Pt-O_2 bond distance, Å	2.00	2.06	2.04
Pt-N_1 bond distance, Å	2.09	2.06	2.06
Pt-N_2 bond distance, Å	2.09	2.06	2.04
O_1-Pt-O_2 bond angle, ^{o}	83.6	81.0	82.5
O_1-Pt-N_1 bond angle, ^{o}	96.3	98.3	96.0
O_1-Pt-N_2 bond angle, ^{o}	178.9	179.2	175.6
O_2-Pt-N_1 bond angle, ^{o}	179.9	179.2	169.7
O_2-Pt-N_2 bond angle, ^{o}	97.4	98.2	98.6
N_1-Pt-N_2 bond angle, ^{o}	82.6	82.5	83.8

Table 2. Calculated total energies of aquated and hydroxylated Pt-DACH complexes.

Complex	Relative energy, eV (w/o PCM corrections)	Relative energy, eV (w/ PCM corrections)
H_2O-(Pt-DACH)-H_2O	0.00	-8.39
H_2O-(Pt-DACH)-OH	+6.84	+3.95
HO-(Pt-DACH)-OH	+8.06	+6.62

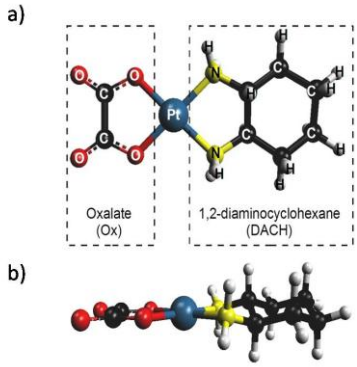

Fig. 4. Calculated structure of oxaliplatin. a) Top view. b) Side view.

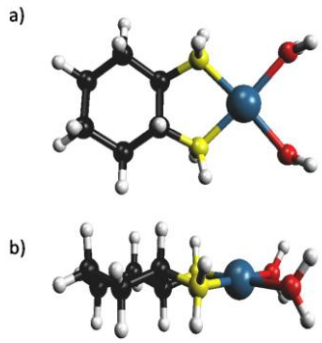

Fig. 5. Calculated structure of the Pt-$(H_2O)_2$DACH complex. a) Top view. b) Side view.

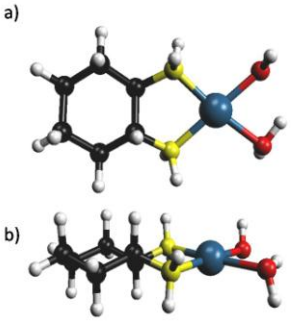

Fig. 6. Calculated structure of the Pt-(H_2O)(OH)DACH complex. a) Top view. b) Side view.

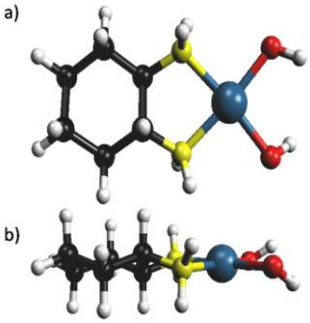

Fig. 7. Calculated structure of the Pt-$(OH)_2$DACH complex. a) Top view. b) Side view.

Another hydrolysis mechanism we consider is one that does not involve hydroxyl groups. While the formation of NH^- in the presence of a nearby –COOH is normally not favorable in solution, we think that the presence of Pt in the structure of the first oxaliplatin hydrolysis product [Pt-Ox(H_2O)DACH] (Fig. 8) could make a difference. The structure of the transition state (Fig. 9) shows the ring opening of the Ox ligand, abstraction of a hydrogen atom from the -NH_2 group of DACH, and the binding of an H_2O molecule to Pt. In contrast to the previously proposed oxaliplatin hydrolysis mechanism, the transition state calculation shows that a hydrogen is not abstracted from the water ligand that binds to Pt. Rather, the water ligand remains intact, but the hydrogen is abstracted instead from a nearby -NH_2 group of the DACH ligand by an oxygen atom belonging to the oxalate group. The proton abstraction is made feasible by the orientation of the oxalate group, which lies almost perpendicular to the DACH ligand but tilted towards the -NH_2 group of the DACH ligand. The activation energy (Table 3) for the forward reaction (from oxaliplatin to the transition state complex) is only 0.41 eV, indicating a high possibility that the proton travels from the -NH_2 ligand to the O atom of the oxalate group. The activation energy for the reverse process [from Pt-Ox(H_2O)DACH to the transition state] is in the same range, at 0.45 eV, which suggests the possible reversibility of the reaction in question.

Table 3. Comparison of calculated values for oxaliplatin, the Pt-Ox(H_2O)DACH complex and the transition state.

Parameter	Oxaliplatin (w/o PCM corrections)	Oxaliplatin (w/ PCM corrections)	TS	Pt-Ox(H_2O)DACH (w/o PCM corrections)	Pt-Ox(H_2O)DACH (w/ PCM corrections)
Pt-O_2 distance, Å	1.999	2.057	3.280	N/A	N/A
Pt-OH_2 distance, Å	N/A	N/A	2.176	2.242	2.247
O_2-Pt-OH_2 angle, ^{o}	N/A	N/A	119.0	N/A	N/A
O_2-Pt-N angle, ^{o}	179.9	179.2	51.9	N/A	N/A
OH_2-Pt-N angle, ^{o}	N/A	N/A	170.7	172.3	177.2
Relative energy, eV	0.00	-1.97	+0.41	-0.04	-2.18

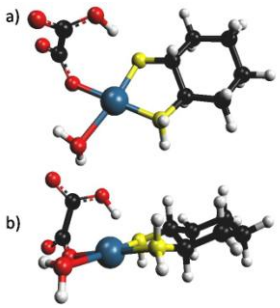

Fig. 8. Calculated structure of the Pt-Ox(H_2O)DACH complex in which the Ox ligand has undergone ring opening and abstracted a hydrogen atom, and in which a water molecule is now bound to Pt. a) Top view. b) Side view.

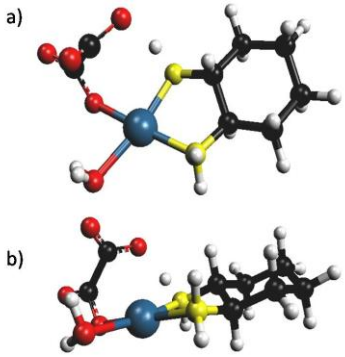

Fig. 9. Calculated transition state structure of the first hydrolysis step. a) Top view. b) Side view.

In the calculated structures containing guanine, namely the Pt-G(Ox)DACH complex (Fig. 10) and the Pt-G(H_2O)DACH complex (Fig. 11), the G molecule lies twisted relative to the

DACH ligand plane. This is not unexpected since the twisted orientation of the two fused-ring ligands would minimize steric repulsion and stabilize the complex.

The calculated structure of Pt-G_2DACH presented in the current work (Fig. 12), in which the two G ligand planes are twisted upward and downward relative to the Pt-DACH plane, is similar to those measured in both the solution and crystal phase. Calculated bond angles (Table 4) share a higher degree of similarity to those of the solution-phase measured by NMR, lending credence to the hypothesis that the differences in the experimentally determined structures in the solution-phase and crystal structures arise from the crystal packing constraints. The calculated structure corresponds to a single Pt-G_2DACH molecule, for which crystal packing forces are absent. The calculated bond angles would thus be expected to be similar to those of the solution-phase structure, which also does not have crystal packing effects.

The calculations also suggest that the environment of the Pt-G_2DACH complex in solution does not exert any significant effect on the structure of the complex since the calculated and measured solution phase bond angles are quite similar. The calculated structure involves only an isolated Pt-G_2DACH complex, while the solution phase NMR studies investigated the structure of an oxaliplatin bound to two G molecules via an intrastrand cross-link in a DNA dodecamer duplex in solution. But in the crystalline phase, it is possible that packing the DNA fragment with the Pt-backbone gives rise to additional crystal packing constraints, which must be sufficiently large to cause the bond angles to deviate from the corresponding bond angles measured in solution. As mentioned earlier, the corresponding cisplatin complexes also have solution phase structures that differ from those in the crystalline phase.

Table 4. Calculated and experimental bond angles for Pt-G_2DACH complex. N refers to the nitrogen of DACH, while NB refers to the nitrogen of guanine bases.

Bond angle	Calculated (w/o PCM corrections)	Calculated (w/ PCM corrections)	Expt'l (NMR)	Expt'l (X-ray)
N_1-Pt-N_2	82.7	82.9	85.7	84.0
N_1-Pt-NB_1	93.5	94.1	91.9	79.6
N_2-Pt-NB_2	93.5	94.0	92.0	97.8
NB_1-Pt-NB_2	90.4	89.2	90.9	98.4

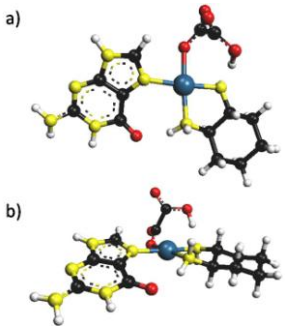

Fig. 10. Calculated structure of the Pt-G(Ox)DACH complex. a) Top view. b) Side view.

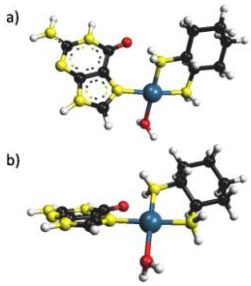

Fig. 11. Calculated structure of the Pt-G(H_2O)DACH complex. a) Top view. b) Side view.

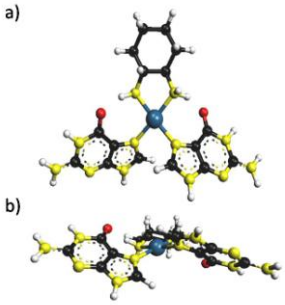

Fig. 12. Calculated structure of the Pt-G_2DACH complex. a) Top view. b) Side view.

In summary: theoretical investigations involving the hydrolysis of oxaliplatin show two possible mechanisms:

1) Through the formation of hydroxyl complexes and
2) Through intramolecular proton transfer during the ring-opening step of Ox while water attacks platinum.

Also, calculations involving the structure of Pt-G_2DACH agree well with those obtained by NMR in solution phase. It thereby supports the possibility of crystal packing constraints having a substantial effect on structural parameters in the solid phase. The calculations also suggest that the environment of the Pt-G_2DACH complex does not exert any significant effect on structure in solution phase.

Life as a QED-C Short Term Program Student

Being a researcher has its share of benefits. Aside from being able to learn much about our chosen field of study from other capable practitioners, we also interact amongst ourselves not only academically, but also socially. We organize activities designed to foster inter-cultural relations, one of these being…

…the International Food Festival!

Thanks in part to the ample remuneration provided by the program, we students are also able to not merely stay in Japan, but to *experience* it.

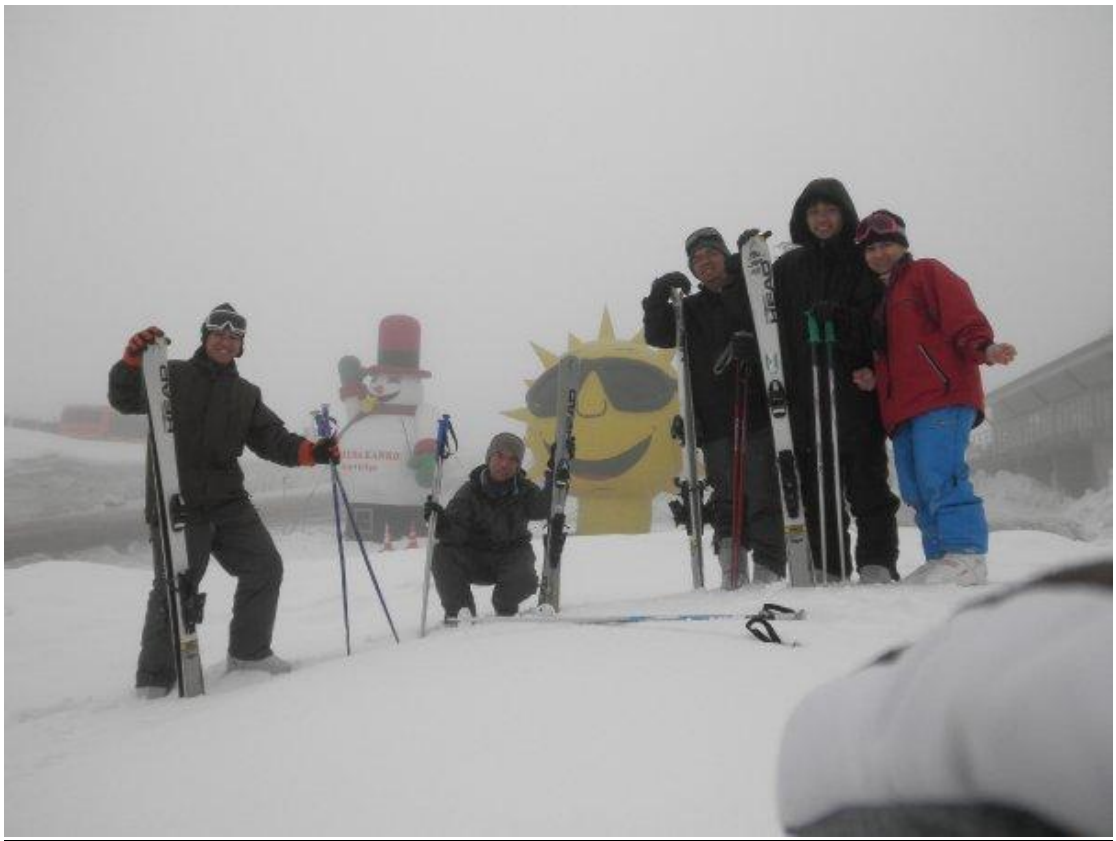

スキー@赤倉観光リゾート

天神祭り

Of course, the Osaka University experience would not be complete without this gratuitous campus shot:

桜@阪大

Truly pictures worth thousands of words. Images encapsulating indelible memories.

Studies on Crystal Surface Defects: Effects to Surface Chemical Reactions and Surface Electronic Properties

*Francisco C. Franco Jr., Prof. Michio Okada[a], Prof. Toshio Kasai[b], Prof. Hikaru Kobayashi[b], and Daichi Yamazaki[a]

** Quantum Engineering Design Course Special Research Student (12months), Osaka University, Oct. 2009-Sept. 2010*
De La Salle University – Manila, Philippines
[a] Renovation Center of Instruments for Science Education and Technology, Osaka University
[b] Institute of Scientific and Industrial Reseach, OsakaUniversity

Abstract

My research as a QED 1-year student was mainly about the properties and effects of defects on crystal surfaces. Gas-surface reactions of ethylene to Cu(210) and Cu(410) were studied using Infrared Reflection-Absorption (IRAS) and Temperature Programmed Desorption (TPD) experiments. Extending the study to materials science, I did experiments on the stability of the HNO_3 passivation method to Si(111) and Si(100) substrates by Microwave-Photoconductance Decay (μW-PCD) method.

---

1. Introduction

In a perfect crystal, all host atoms are located on their proper lattice sites and the crystal contains neither impurities nor structural imperfections.[1] However, due to thermodynamic considerations, a perfect crystal is impossible to achieve thus requiring certain amount of structural defects. Some defects are unavoidable, while others are process-dependent.

Unfortunately, it is very difficult to analyze the properties of materials due to random and irregular defects. Thus, to approximate these defects, it will be helpful to study systems with well-defined defects. To aid in the study of well-defined defects, I did experiments on the gas-surface adsorptions of Cu(210) and Cu(410) and extended it to the surface passivation of Si(111) and Si(100).

To approximate the defect sites for ideal surfaces to that of heterogeneous catalysts for practical use, surfaces with higher-Miller index faces like (210) and (410) can be used due to the presence of well-defined defects (Figure 1) such as the terraces and steps in order to analyze more complicated systems.

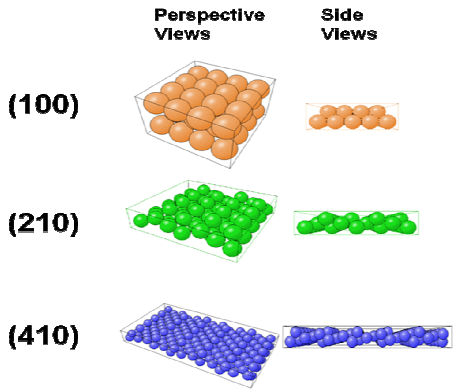

Figure 1: Perspective and side views of the (100), (210) and (410) faces.

The study of defects can also be applied to the field of photovoltaic devices. Solar cells generate electricity by the absorption of light. The electron-hole pairs then generate a potential difference which then generates electricity (Figure 2)[2].

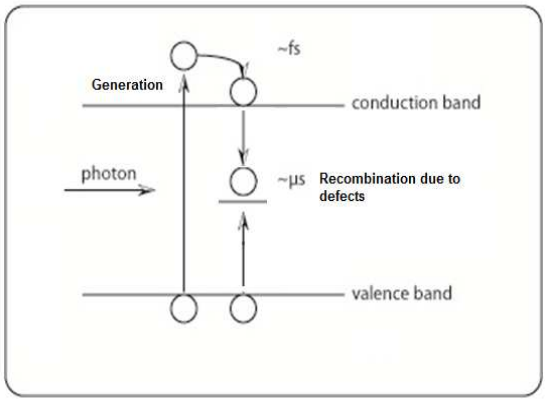

Figure 2: Mechanism for electron-hole pair generation of photovoltaic devices

Therefore, it is very important that we limit the recombinations of these electrons and holes for more efficient solar cells. Since most recombinations occur on the surface, an effective surface passivation is thus required. Thermal oxidation of silicon, by far, is one of the most effective methods for reducing surface recombinations. However, this method introduces stress to the silicon substrate which may result to the degradation of the bulk lifetime. Thus, a low temperature passivation method is required for the improvement of solar cells.

2. Experimental

2.1. Ethylene Adsorption experiments

The experiments were performed in an ultra-high-vacuum (UHV) chamber pumped down to a base pressure of 4.0 x 10^{-8} Pa with a turbo-molecular pump and a titatinium sublimation pump. A schematic view of the apparatus is shown in Fig. 3. The chamber is equipped with a Fourier-transform infrared (FTIR) spectrometer, a mercury-cadmium-telluride (MCT) detector, a quadrupole mass analyzer (QMS) and a low-energy electron diffractometer (LEED).

A mechanically polished single crystal surface (15 mm x 15 mm x 0.7 mm, Surface Preparation Laboratory) Cu(210) and a 10 mm Cu(410) diameter disk cut within 0.1° from the 410 plane were used for the measurements. The clean surfaces were prepared by several cycles of Ne ion bombardment (1 keV, 2.2 µA/cm2, 30 min) and subsequent anneals at 700 K or 900 K for 5 min.

IRAS spectra were recorded using FTIR spectrometer (JASCO FT/IR 6100) with a liquid

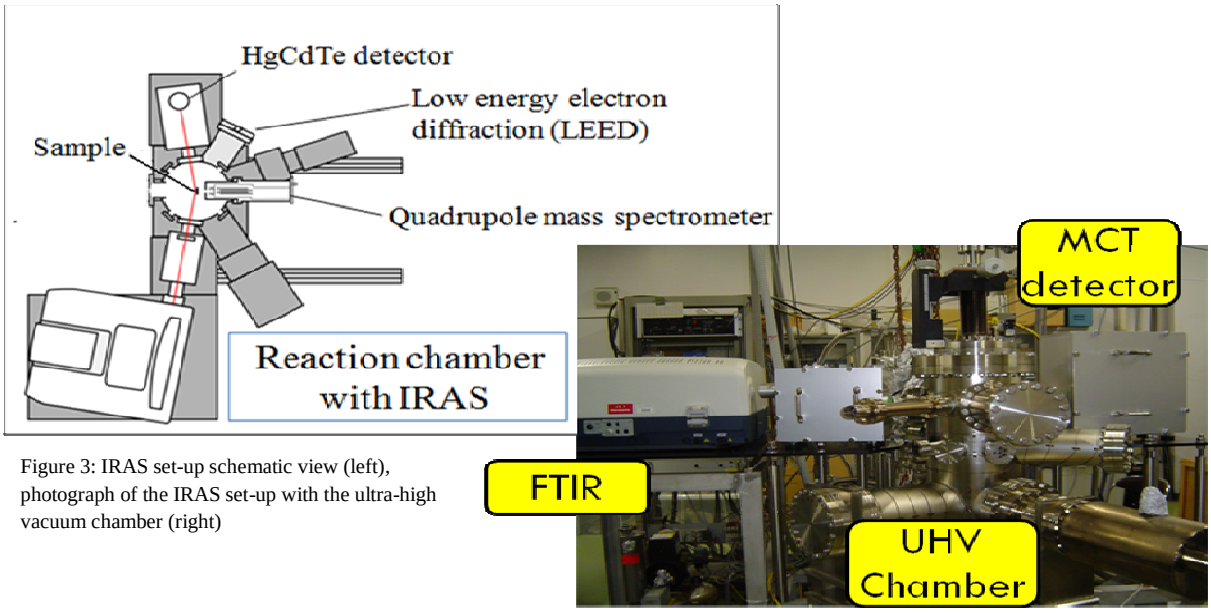

Figure 3: IRAS set-up schematic view (left), photograph of the IRAS set-up with the ultra-high vacuum chamber (right)

nitrogen cooled HgCdTe (MCT) detector. The spectral range lies between 800 cm^{-1} and 3500 cm^{-1}, although truly stable operation is difficult below 950 cm^{-1}. Spectral resolution was 4 cm^{-1} and around 512 scans were typically collected. The incident IR beam was p-polarized with a wire grid polarizer and focused through a BaF_2 window onto the sample surface at an incident angle of 80° off normal. A dried air generator (Paker BALSTON 75-62JA) was used for the purge of all optical paths and the interferometer.

Temperature-Programmed Desorption (TPD) measurements were carried out with QMS (Leda Mass Ltd. Microvision) enclosed by a random-flux shield. To maximize the signal of desorbing molecules during TPD, the sampling orifice of the QMS was positioned within 2 mm away from the Cu(210) sample. The sample was cooled down with liquid nitrogen and exposed to ethane or CO by backfilling the chamber with high purity.

2.2. Surface passivation experiments

Figure 4 shows the preparation of the silicon wafers for lifetime measurements. Two sets of four different wafer types (45 x 45 mm) were used as substrates for the passivation treatments: p-type and n-type Si(100) with resistivities in the range of 1-20 Ω·cm, p-type and n-type Si(111) with resistivities in the range of 3.00 – 5.00 Ω·cm and 1.00 – 3.00 Ω·cm respectively.

All the samples were cleaned by the RCA (Radio Corporation of America) cleaning process (where: RCA-1 = 1:1:5 ratio of NH_4OH: H_2O_2: H_2O and RCA-2 = 1:1:5 ratio of HCl: H_2O_2: H_2O) followed by rinsing in deionized water. After cleaning, the samples were etched in (0.5%) dilute hydrofluoric acid. One set of wafers were immediately measured for their lifetimes using the Microwave-Photoconductive Decay (μW-PCD) machine (KOBELCO Wafer-T LTA-1510).

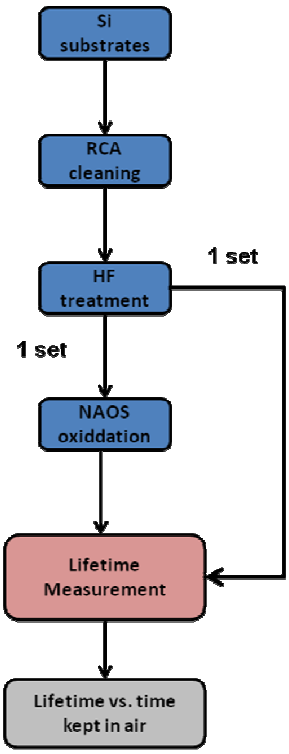

Figure 4: Preparation process of silicon substrates for lifetime measurements

In the μW-PCD method (Figure 5), excess carriers are injected by the irradiation of the surface of a silicon wafer with pulsed laser light. The decay process is detected using 9.6 GHz of microwaves and the laser diode photon flux used was λ = 904 nm, level 2 = 5.0 x 10^{13} photons /cm^2. The penetration depth of the laser is about 30μm.

The remaining wafers were then oxidized after HF etching. HNO_3 oxidation was done by inserting the specimens in a quartz glass tube and then heating at temperatures between 100 and 200 °C. Vapor generated by boiling of a 98 wt% HNO_3

solution was introduced into the quartz glass tube and the oxidation was performed at 100-200°C for 5 minutes.

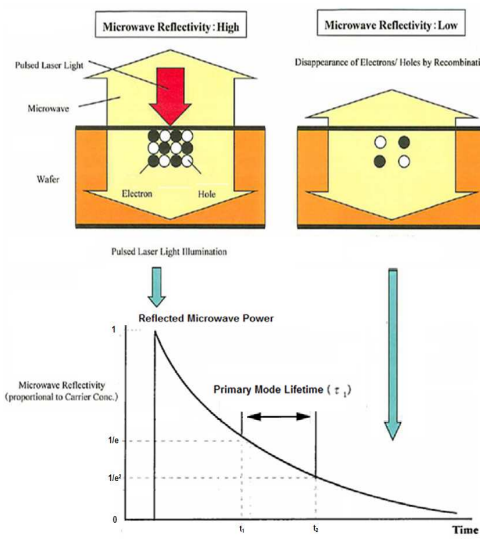

Figure 5: The Microwave Photoconductive Decay method for lifetime measurements

3. Results and Discussion

3.1. Cu(210) and Cu(410)

3.1.1. TPD

The TPD spectra for varying ethylene dosage on Cu(210) were shown in Figure 6. Exposures were reported in units of langmuirs (L) where 1 L equals 1.33 x 10-4 Pa·s. The heating rate was 2.1 K/s and the intensity of m/e = 27 $(C_2H_3)^+$ signal was monitored, since the signal exclusively originates from ethylene. At 0.1 L of exposure, a symmetrical peak at 145 K was observed. As the dosage was increased to 0.5 L and 0.7 L, the peak maximum shifted down to 121 K and the peak shape became unsymmetrical. At dosages greater than ~0.7 L, a second peak appears at around 90 K. The first peak almost didn't further decrease to lower temperatures. Both of the peaks were assigned to π-bonded ethylene since species desorbing at 90 K to 185 K were typically assigned for ethylene keeping their π-nature for Cu surfaces.

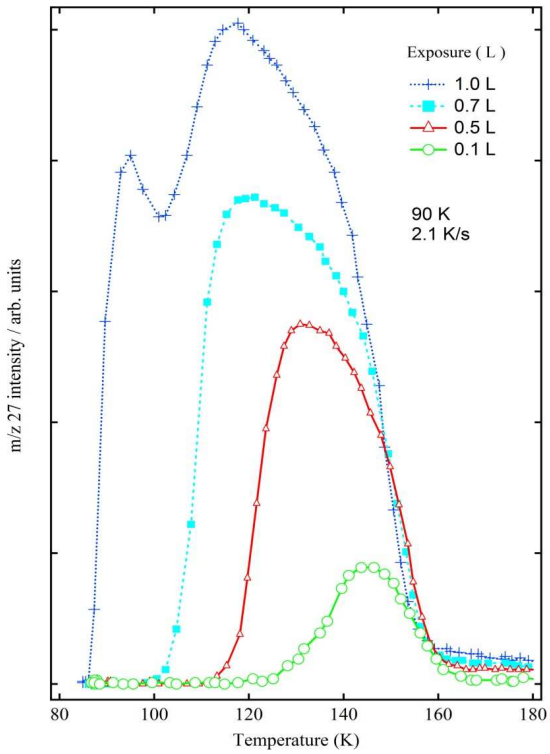

Figure 6: Dosage dependent Temperature Programmed Desorption spectra of ethylene on Cu(210) at 90 K surface temperature and 2.1 K/s

3.1.2. IRAS

To further investigate the nature of the ethylene species on the Cu(210) surface, IRAS measurements were performed for ethylene-Cu(210). The IRAS spectra of Cu(210) at 90 K, 110 K and 145 K are shown in Figure 7. At 145 K only the signal at 932 cm^{-1} was observed and it was attributed to the CH_2 wagging vibrational mode. As the surface temperature was decreased to 110 K, two other peaks at 1549 cm^{-1} and 1287 cm^{-1} were observed. These peaks correspond to the C=C stretching and the CH_2 scissors vibrational modes respectively. As the temperature was further decreased to 90 K, the peak areas of those assigned

to the C=C stretching and CH_2 scissors were observed to increase while the peak area for the CH_2 wagging mode was essentially unchanged. The C=C stretching signal position indicates that there exists only very weak interaction between the ethylene molecule and the Cu surface since the peak position is almost the same as the free ethylene molecule. These data supports the idea that there are at least two adsorption geometries for ethylene on Cu(210) and that there are only π-bonded ethylene and no other vibrational modes corresponding to di-σ bonding (C-C, 1150 cm^{-1}) were observed.

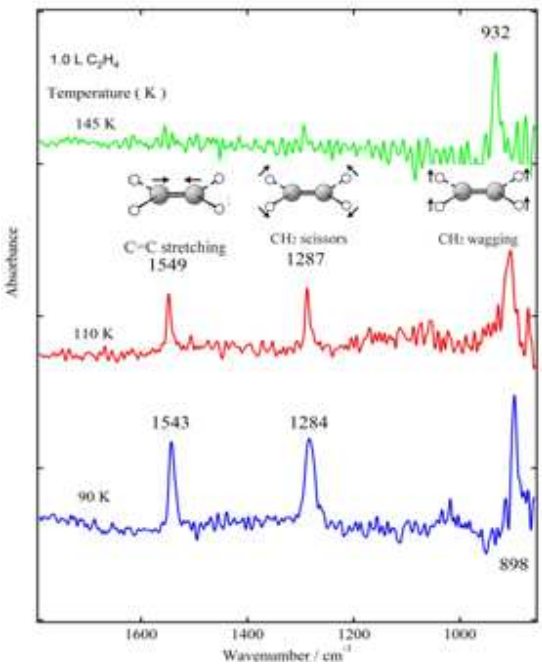

Figure 7: IRAS spectra for 1.0 L of ethylene dosed on Cu(210) at varying surface temperatures of 145 K, 110 K and 90 K.

3.1.3. Cu(210) vs. Cu(410)

In Cu(410), as previously reported by another group[3], it was observed that at 145 K ethylene on Cu(410) only has π-bonding character. Thus, di-σ-bonded ethylene might be initially absent on the surface. But at a higher dosing temperature of 193 K, it was observed that most of the bonded ethylene species were desorbed and the surface was mostly populated with di-σ-bonded ethylene. Subsequently, the di-σ-bonded ethylene was found to undergo complete dehydrogenation.

The decrease in reactivity of Cu(210) as compared to Cu(410) can be attributed to the increase in step density. Due to the decrease in the widths of the terraces, the formation of di-σ-bonded ethylene on the surface will be hindered since desorption of the π-bonded species will be more favoured. Ethylene was previously reported to adsorb at the short bridge site along the <110> direction on Cu(110)[4] and on 4-fold hollow site on Cu(100). Even though the Cu(210) consists of (110) terraces and (100) steps, the width of these sites are too narrow for ethylene to be adsorbed to.

3.2. Si(111) and Si(100)

Figures 8 to 10 show the μW-PCD data for Si(111) and Si(100) for both p-type and n-type for diluted hydrofluoric acid (HF) and nitric acid oxidation of silicon (NAOS) treatments for about 20 days. Initially the HF passivation method is significantly better than the NAOS passivation method as seen from the lifetime values, but as both wafers from the two treatments were exposed to air for long periods, the HF treated ones started decreasing rapidly before becoming stable after 2 days. After 20 days for n-types: in Si(111), NAOS is 14% better than HF treatment, while in Si(100), NAOS is 45% better than HF treatment. On the other hand for p-types: in Si(111), NAOS is 3% better than

HF, while in Si(100), NAOS is 8% better than HF treatment. These results are consistent with the fact that the H-terminated surfaces for silicon since H-Si bonding is known to be easily be cleaved and oxidized, while for NAOS treatment, it was shown previously[5,6] that silicon wafers oxidized by high concentrations of nitric acid vapour, forms a very dense SiO_2 layer on the silicon substrate.

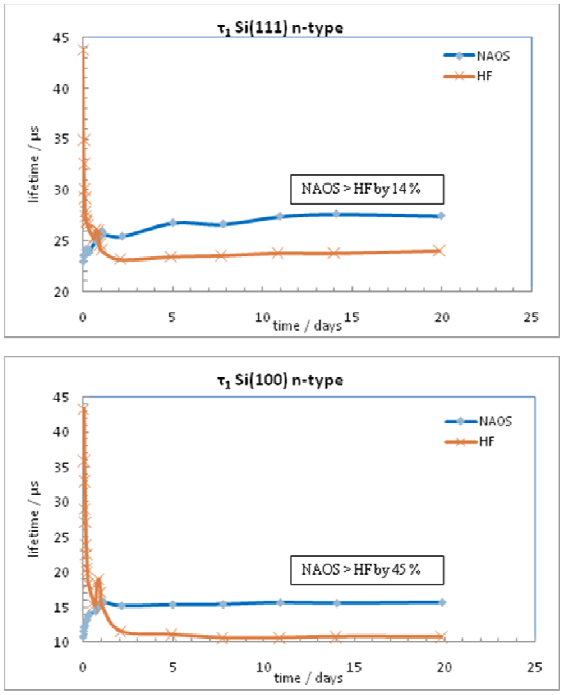

Figure 8: µ-PCD lifetime trends for the n-types of Si(111) (top)and Si(100) (bottom) for both NAOS and HF passivation methods

Figures 8 to 10 also shows that in n-types for both Si(111) and Si(100), initially the NAOS treated ones were still increasing after the initial treatment before becoming stable. While for p-types, it can be observed that the lifetimes of the NAOS treated wafers decreases after the initial treatment before stabilizing at long exposure to air. This observation can possibly be correlated to the incomplete oxidation after the initial treatment of the silicon wafers and the oxidation continuing even after the treatment for about 1-2 days.

Another trend that can be observed from the graph is the increase of the lifetimes for the HF-passivated wafers 16-18 hours after the initial treatment. This is quite a surprising since it was known that the lifetimes of HF passivated silicon wafers decreases rapidly after the treatment and was thought to just flat out after long exposure to air. And also, comparing the increase to the surface orientations of the silicon wafers, it can be seen that the Si(100) wafers have higher increase than Si(111). It is possible to attribute this observation to the HF-passivated wafers being slightly stabilized by the oxide layers produced since it can be readily oxidized during the H-Si bond cleavage and Si(100) was previously observed to have a faster oxide growth rate than Si(111) due to the greater atomic distance for the Si(100) surface (1.45 Å) than Si(111) surface (1.04 Å).

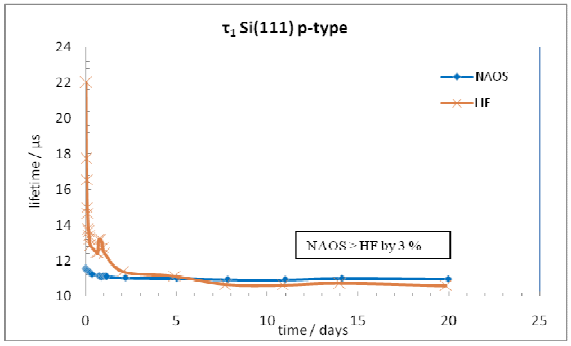

Figure 9: µ-PCD lifetime trends for p-type Si(111) for both NAOS and HF passivation methods

Considering the doping types, it can be seen that the lifetimes for n-types for both Si(111) and Si(100) have longer lifetimes after 20 days as compared to p-types. The minority carriers in n-type wafers are the holes which are widely known to have higher lifetimes as compared to electrons

as the minority carriers in p-type materials[7]. Phosphorus doped silicon wafers as reported, can mitigate recombinations associated with chemical and crystallographic defects[8]. They demonstrated that n-types have lower recombination rates in the following cases: (a.) laser induced dislocations, (b.) different surface passivation methods, and (c.) contaminated wafers.

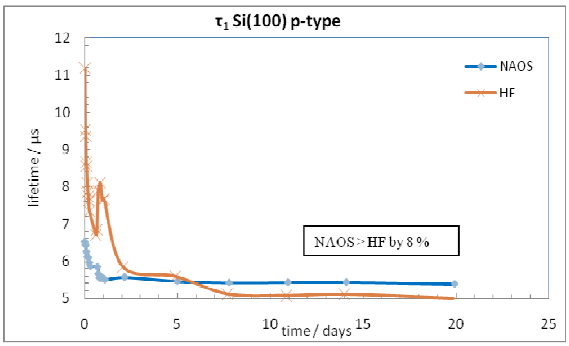

Figure 10: µ-PCD lifetime trends for p-type Si(111) for both NAOS and HF passivation methods

Comparing the lifetimes of the silicon wafers based on surface orientation, the figures show that (111) surface orientation have higher lifetimes than (100) oriented surface for both passivation methods. Three key points that may help explain these results were proposed by Angermann *et. al.*[9] after determining the surface interface state densities during each step of the RCA cleaning and HF/NH_4F etching processes: (a.) surface state density of Si(100) is higher than that of Si(111) as observed from their SPV and SE measurements, (b.) Si(111) surface can be modelled as having only one dangling bond per atom while the Si(100) surface can possibly have two dangling bonds or adatoms, and (c.) faster oxide growth for Si(100) than Si(111) due to the greater atomic distance on the (100) surface than (111).

4. Conclusion

The main theme of my research as a 1-year QED student was mainly on defects and their effects on surface properties. Infrared Reflection-Adsorption spectroscopy and Temperature Programmed Desorption measurements were used to determine the surface reactivity of ethylene on Cu(210) and Cu(410). It was found that ethylene is not as reactive on Cu(210) as compared to Cu(410) and it has two bonding geometries on the Cu(210) surface while retaining most its π-bonding character. For the application related study, the Microwave Photoconductance Decay method (µ-PCD) was utilized for the determination of the stability of surface passivation for both nitric acid oxidation of silicon (NAOS) and HF passivation methods. It was found that NAOS is a better passivation method as compared to HF treatment for long exposure to air and that n-type wafers have longer lifetimes than p-types.

5. Acknowledgements

I am sincerely grateful to the Quantum Engineering Design course, a joint project of JASSO and ASEAN, for giving me the opportunity to expand my knowledge in the field of science and engineering. I would like to thank Dr. T. Kasai, Dr. M. Okada, Dr. M. Hashinokuchi, Dr. H. Kobayashi, Dr. W.B. Kim, Dr. H. Kasai and Dr. W. Dino for all the advice/support before and during my stay and for all the research opportunities in Osaka University. I also would like to thank some students: Mr. Yamazaki, Mr. Kanda and Mr. Nakamura who really helped me a lot in doing research and adjusting to the Japanese life. Finally, I would like to thank the secretaries: Tanaka-san, Nojiri-san, Hosokawa-san and Kurozaki-san for all the advice and help in the processing of my documents during my 1-year stay.

6. References

[1] O'Mara, Handbook of Semiconductor Silicon Technology, NOYES Publications, 1990

[2] J. Nelson, The Physics of Solar cells, Imperial College UK, 2003

[3] T. Kravchuk, *et. al.* J. Phys. Chem. C. Vol. 113, No. 49, 2009 20883

[4] J. Buisset, *et. al.* Phys. Rev. B. 1996, 54, 10373

[5] W.B. Kim, *et. al.* Journal of Applied Physics, 105, 103709 (2009)

[6] W.B. Kim, *et. al.* Nanotechnology, 21, (2010), 115202

[7] J. Zhao, et. al. Photovoltaic Specialists Conference, 2002. Conference Record of the Twenty-Ninth IEEE, May 2002, 218-221

[8] J.E. Cotter, *et. al.*, IEEE Transactions on Electron Devices, Vol. 53, No. 8, Aug. 2006

[9] H. Angermann, *et. al.* Materials Science and Engineering B73 (2000) 178-183

My Japan Life Experience

Before I arrived in Japan, I had some really nice expectations regarding the Japanese life, culture and people. After 12 months of staying in Japan, I'm very happy to say that most of my expectations were mostly right. Although I can say that I'm already quite used to and comfortably living in Japan, there are still times when I get excited/surprised/shocked with what I see/experience. Maybe for first timers, everything in Japan seems so complicated due to language and reading barriers (Kanji) but as I get used to living in Japan, I realized that everything's systematic and living in Japan is really quite easy although I have to say, it's so expensive to live in Japan.

Figure 1: Autumn in Kyoto

It took me about two weeks before I got used to living a different life. But as time goes by, I learned to enjoy the things that seemed so difficult or different from what I was used to: like walking a lot, being able to ride a bicycle everywhere (e.g. to namba from satsuki-gaoka), food, riding trains and buses, hearing and reading Japanese, seeing so many Nihon-jins and other foreign people every single day of my life. But before I knew it, I was already having a great time.

Figure 2: Skiing in Niigata

From my stay in Japan, I can say that my most exciting experience was when I went to Niigata, in Akakura onsen to do skiing (I'm a sports enthusiast!). It was really difficult at first but as I got used to wearing those long skis and big boots, it became really, really exciting. Slowly, I tried more difficult courses and when finally I tried the very long and steep course, it was really rewarding because the trees at the top of the slope were really different together with the appearance of snow and of course the thrill and excitement I felt as I go down the slope. I also like going to public baths/onsen because I really feel good when I warm up my body. I also went to some places like Kyoto, Kobe, Okazaki, and Fukuoka to name a few and I can say that I really enjoyed the sceneries and my stay when I went to those places. I also went to a couple of matsuris which is really nice, since I was able to see girls wearing kimonos which I find really cute.

Figures 1-4 demonstrates *me* during the four seasons here in Japan. It was really nice to experience the four seasons since we only have summer and rainy seasons in the Philippines, although, I really didn't like the winter. It was really difficult for me to go outside!

Of course one of the things that I really loved about Japan is the food since I really love to eat. Of course, sushi ga daisuki! Unagi is my favourite followed by salmon, and next are all the rest of the sushis (including nato). It was really fun eating in kaiten sushis where I get to pick up 105yen sushi plates. Also, I love the rice cakes, the sweet and sticky balls. Then, there's also the different kinds of noodles especially yakisoba (it's so different compared to the Philippines). And then there are also the tabehodai restaurants, which is really good after a good bicycle workout. I also like using chopsticks for eating, although I don't know why but still it feels good.

Figure 3: Spring in Minami Senri park, under the Sakura tree (wearing a la sale shirt)

But, the best thing I liked during my stay here in Japan is meeting people from many different countries and of course the Nihon-jins. It was really nice to learn more about other cultures and to learn many different ideas from people you've only met for a short time. I really felt like I'm having one of the best parts of my life because these are the things that I might never get to experience again and I'm doing all of them mostly all by myself so I know that my personality/experience really grew from my stay here because I learned lots of invaluable lessons in life from all the people I met and the things I experienced.

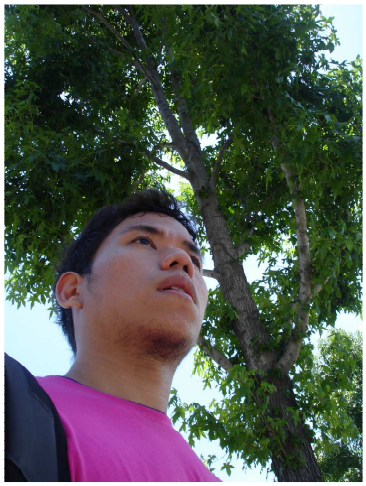

Figure 4: Summer in Fukuoka

For my final words, I really would like to thank QED for giving me an opportunity to grow as a scientist and as a person. I'll always treasure everything I experienced, because Japan will always be in my heart. I also would like to thank all the people I met in Japan (senseis, students, friends, staffs, locals, etc.) for letting me become a part of their lives and them being a part of mine.

I'll forever be grateful for my 1-year Japan experience. It was a blast!
Arigatou gozaimashita.

Sayonara,

Francisco C. Franco Jr.
QED 1-year Research Student
De La Salle University – Manila Philippines

Quantum Engineering Design Course Report

Adsorption of O_2 on Fe-(n)pyrrole Molecules from First-Principles Calculations

Hani Fadinna[1,2], Hermawan K. Dipojono[1], Adhitya G. Saputro[2], Hideaki Kasai[2]

[1] Laboratory of Computational Materials Design, Research Group of Engineering Physics, Institut Teknologi Bandung Jln., Ganesha 10, Bandung 40132, Indonesia [2] Department of Precision Science and Technology and Applied Physics, Osaka University, Suita, Osaka 565-0871, Japan

Abstract

The research of Los Alamos National in synthesizing Fe-polypyrrole-Carbon [1)] as non-precious metal catalyst is gives challenge to find another commercially viable and alternative catalyst for fuel cell. Inspired by the previous work of adsorption of O_2 on Co-(n)pyrrole cluster [2)], this study will investigate interaction of O_2 molecule with new non-precious catalyst namely Fe-polypyrrole which is expected to have good activity in oxygen reaction reduction. In this study we performed a DFT based calculation on the adsorption of O_2 molecule on Fe-(n)pyrrole cluster using Gaussian 03 [3)]. The hybrid functional B3LYP was employed for the exchange-correlation energy and 6-311+G(d,p) basis-set was used for the basis function. The stable adsorption site of O_2 molecule on Fe-(4)pyrrole is found to be at the O_2 center of mass located on the top of the Fe atom.(side-on configuration) while Fe-(6)pyrrole at-end on configuration The elongation mechanism of O_2 on Fe-(n)pyrrole is induced by the interaction between the Fe d-orbitals and O_2 anti-bonding π^* orbital, which results in charge transfer from Fe atom toward the O_2 molecule.

Introduction

PEM fuel cell using hydrogen as it fuel is one of promising device for energy converting but currently it has a number of issues related to the cost[4)]. Until now, fuel cell is still fairly limited to reach economic market due to the expensive of fuel cell itself. One of the most expensive factors is a platinum catalyst used in both cathode and anode of the fuel cell. In reality during the PEM fuel cell operation 45 percent of catalyst can be lost in five days[5)] because the kinetic reaction of oxygen reaction reduction (ORR) at the cathode side during PEM fuel cell operation is slower than the hydrogen oxidation reaction at the cathode side.

Inspired by iron-porphyrin as organic compound hemoglobin that contains four pyrrole rings to bind the metal Fe which have responsible for binding the oxygen, now recently a researcher has synthesized a possible development of Fe[6,7)] and Co based catalyst[6,8)]. Bahsyam and coworker[8)] has developed a cathode catalyst using non platinum based catalyst and made from a cobalt-polypyrrole-carbon composite which exhibiting high ORR activity with stable performance. Following this Lefèvre and coworkers[7)] used active

iron cation coordinated to pyridinic groups within micropores of the carbon support and notes that after extended use in a fuel cell, the catalyst's high initial activity decrease significantly.

In this work, density functional calculations were performed to determine a possible model for Fe-polypyrrole and hence to understand the interaction of O_2 molecules on Fe-polypyrrole cluster to clarify the oxygen reduction reaction at the cathode side. Following this, another goal was to develop a predictive scale of Fe-polypyrrole reactivity based upon structure, and calculated properties. In the process of carrying out these calculations a number of basis sets were tested.

Computational Method

All of calculation used density functional theory (DFT) methods and were carried out using Gaussian03 package[3]. Initial optimizations and spin ground state species calculation were carried out at the B3LYP/LANL2DZ level. Second calculations used to calculate energy and test these method with employed the larger 6-311++G(d,p) [9].

Natural bond orbital (NBO) [10] population scheme was used to perform of many electron molecular wave function in terms of localized electron-pair bonding unit. This method is based on a method for optimally transforming a given wave function into localized form, corresponding to lone pair and bond elements of chemist's Lewis structure picture. We used NBO population scheme for molecular orbital analysis and atomic charge calculation.

Result and Discussion

We started our theoretical investigation with optimizing Fe-(2)pyrrole cluster as being proposed by Bahsyam et al., [8] for cobalt-polypyrrole-carbon. With regard that Fe atom is in 2+ ionic state, firstly two pyrrole rings are connected with substituting two hydrogen atom as shown in fig 1. (a) where the Fe atom is bonded two N atom as shown in fig 1. (b)

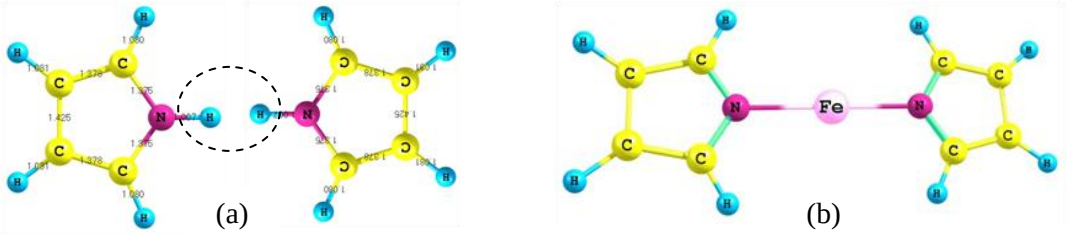

Fig . 1. Sructure of (a) two optimized pyrrole rings (b), optimized Fe-(2)pyrroles

In the process of carrying out these calculations a number of theory levels, basis sets were tested. We consider Fe-(4,6)pyrrole with spin multiplicities of 1, 3, 5, 7 and let it fully relaxed the geometry at each spin state as proposed in ref[2]. The calculated optimized structures of Fe-(3,4,6)pyrrole and their

interaction with O_2 molecule are given in table in Table I. The initial geometry trial for those cluster are difficult to reach energy convergence due to the non-planar structure resulted.

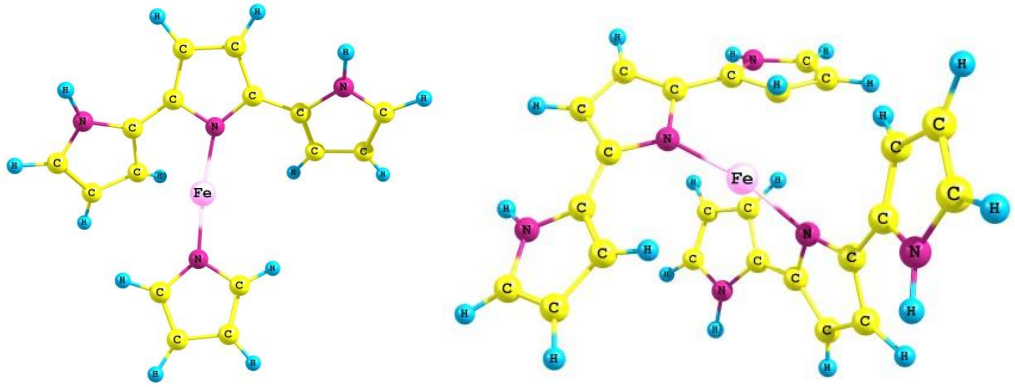

(a) (b)

Fig. 2. Optimized structures of Fe-(4)pyrroles (a) cluster and Fe-(6)pyrrole cluster (b)

The calculated optimized structures of Fe-(3,4,6) and their interaction with O_2 molecule are given in table in Table I. From calculation we found that the isolated Fe(2+) atom has a pentet spin state with spin multiplicity 5 meanwhile Fe on Fe(4)pyrrole and Fe(6)pyrrole are 2.16 and 2.05, respectively . This showed that for both Fe-(4)pyrrole and Fe-(6)pyrrole there is a large change in spin population of Fe atom. Figure 2 (a) and (b) show the optimized structure for both Fe-(4)pyrrole and Fe-(6) cluster are non-planar structured likewise in Co-(4,6)pyrrole cluster case in ref [2)].

In considering another ionic charge 3+ of Fe, we predicted the model for Fe-(3)pyrrole and Fe-(5)pyrrole cluster as shown in Fig. 3. (a) and (b)

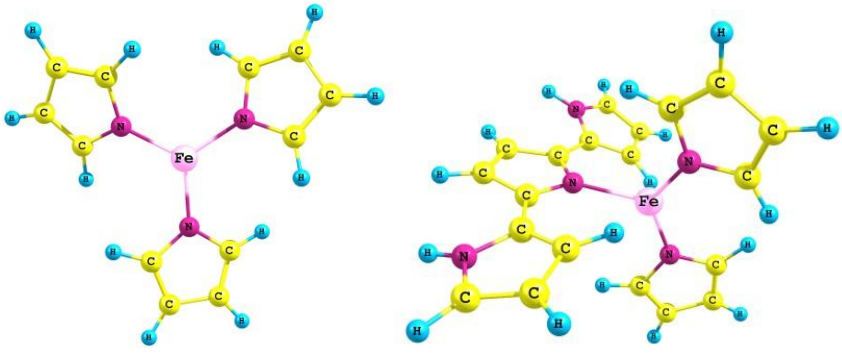

(a) (b)

Fig.3. Final Optimized structured for Fe-(3)pyrrole (a), Fe-(5)pyrrole (b)

Table I. Ground states multiplicities, structurals parameters, vibration frequencies and atomic charges, calculated for different optimized Fe-(3,4,6)pyrrole cluster and for the isolated O_2 molecule.

Molecule	**Spin Multiplicity**	**d(Fe-N) (Å)**	**N-Fe-N (°)**	**d(Fe-O) (Å)**	**d(O-O) (Å)**	**Q(Fe)**	**Q(O2)**	**s(Fe)**	**s(O_2)**	***ν*(O-O) (cm^{-1})**
3-pyrrole-Fe	6	1.91	120	-	-	1.63	-	4.09	-	-
3-pyrrole-Fe-O_2	8	1.99	107.56	1.99	1.31	-	1.64	4.03	1.421	
4-pyrrole-Fe	3	1.91	172.15	-	-	0.96	-	2.16	-	-
4-pyrrole-Fe-O_2	5	2.037	110.19	2.04	1.41	1.11	-0.58	3.73	1.19	988
6-pyrrole-Fe	3	1.94	152.28	-	0.94	-	-	2.05	-	-
6-pyrrole-Fe-O_2	5	1.99	137.53	1.85	1.309	1.09	0.60	2.15	0.86	-

3.1 O_2 Molecule Adsorption On Fe-(4,6)pyrrole

Considering the interaction between Fe-(n)pyrrole with O_2 is a first step to understand and evaluate the prospect of using Fe-(n)pyrrole as an ORR-catalyst. The optimized structure from our calculation for Fe-(4)pyrrole in Fig 4. shown the stable adsorption site of the O_2 molecule on Fe-(4)pyrrole with side-on configuration.

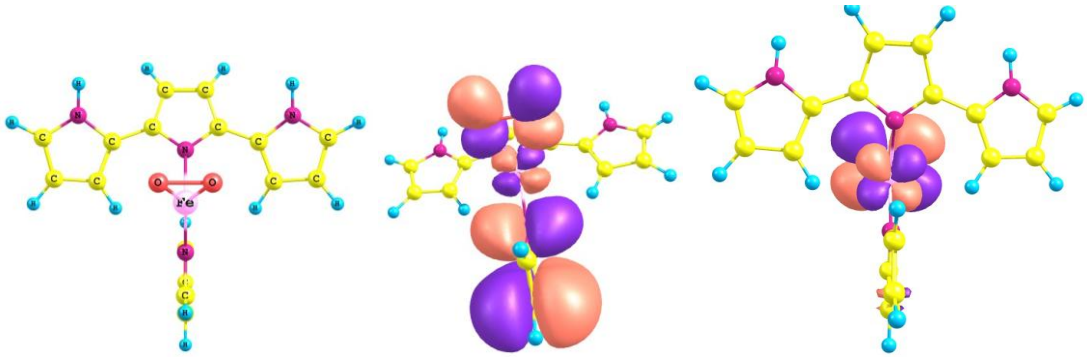

(a) (b) (c)

α HOMO +2 (-5.5 eV) α HOMO 7.07eV

Fig. 4. Side-on interaction of O_2 with Fe-(4)pyrrole (a), the important MOs; HOMO-2 (b) and HOMO-4 for optimized configuration of O_2/Fe-(4)pyrrole.

The side-on interaction in stable distance 2.04 Å gave the adsorption energy 1.69 eV. The interaction of Fe-(4)pyrrole with O_2 molecule bringing the N-Fe-N angel change from 172.15° to 110.19 ° after the optimization due to the strong interaction between the Fe atom and O_2 molecule. From the table, the O-O bond changes when O_2 molecules adsorbed on Fe-(4)pyrrole. Comparing the bond length of an isolated O_2

molecule with the O_2 molecule after it adsorbed on Fe-(4)pyrrole, the O-O bond is elongated by 13.3%. In addition to this, the calculated stretching frequency of the O_2 molecule when it is adsorbed on Fe-polypyrrole is 998 cm^{-1}, which is very different from the isolated O_2 of 1633 cm^{-1}. This elongation of O-O bond and the decrease of O_2 streching frequency after adsorption indicate that O-O bond has been weakened.

To explain the origin of the O-O bond weakening after adsorption, we have checked the molecular orbitals (MOs) for isolated Fe-(4)pyrrole and for the O_2/Fe-(4)pyrrole system. Fig. 4 (b) and (c) shows the calculated MOs for the optimized Fe-(4)pyrrole cluster. It was clear from the features of Fe d-orbitals in α HOMO-2 and α HOMO-4 levels that the side-on configuration is tend to be overlapping of these d-MOs and the O_2 anti-bonding orbital.

Tabel II. Comparison of total valence charge population in O_2 and Fe-(4)pyrrole and for the optimized O_2/Fe-(4)pyrrole system

	Before O_2 adsorption	After O_2 adsorption	Difference
Fe valence orbital population	6.88	6.54	-0.34
4Pyrrole valence orbital population	88.03	87.63	-0.4
O_2 valence orbital population	11.93	12.68	0.75

Table II gives the comparison between the O_2 molecule valence charges populations in 2s and 2p orbitals before and after adsorption, which shows that O_2 has an extra charges of about 0.75*e*. The analysis of the total population indicates that there is a small change in the Fe valence populations, especially in 3d and 4s orbitals, and in the metal and (4)pyrrole valence orbitals populations. The calculated result of table II indicate that the pyrrole is donor the electrons to the Fe at the center of the molecule. From the data, we suggest that the pyrrole rings transfer electrons to the Fe atom, which filled the electrons to the O_2 through the hybridization interaction between Fe-r orbotals and the O_2-anti-bonding orbitals. The origin elongation of O-O bond is mainly causes do to the extra charges in the O_2 molecule. These extra charges would fill the O_2 anti-bonding orbital and weaken the O-O antibonding.

In case of Fe-(6)pyrrole cluster, the O_2 is adsorbed with different configuration from Fe-(4)pyrrole. The steric hindrance effect has occurred and some pyrrole rings try to blocks the pyrrole rings and prevents O_2 to make side-on configuration. As shown in table I, the calculated adsorption energy of the O_2 molecule on the Fe-(6)pyrrole is 0.82 eV with the distance 1.85 eV.

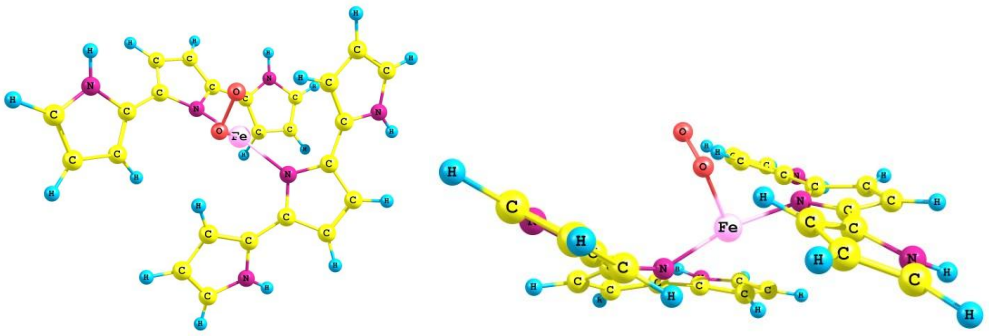

(a) (b)

Fig. 4. End-on interaction of O_2 with Fe-(6)pyrrole, view from the top(a), view from the side (b)

Tabel II. Comparison of total valence charge population in O2 and Fe-(4)pyrrole and for the optimized O2/Fe-(4)pyrrole system

	Before O_2 adsorption	After O_2 adsorption	Difference
Fe valence orbital population	6.88	6.86	0.01
6Pyrrole valence orbital population	131.49	130.82	0.67
O_2 valence orbital population	11.93	12.54	-0.61

3.1 O_2 Molecule Adsorption On Fe-(3)pyrrole

We considering Fe(3+) ionic state and predict the optimized geometries of Fe-(3)pyrrole as shown in Fig.4 (a) The spin multiplicity of Fe-(3)pyrrole has changed after the interaction of Oxygen from 6 to 8 spin state. To optimize this system, firstly we used B3LYP/LANL2DZ level and got the end-on configuration with O-O 8.49% bond elongation, next we refined and recalculated the system using B3LYP/6-311+G(d,p) and it was giving the side-on configuration with O-O bond elongation 9.17%. The molecular orbitals (MOs) for this Fe-(3)pyrrole case also showed that the interaction is dominated by Fe-d orbitals and O_2 anti bonding orbitals as shown in Fig 4(b) and (c).

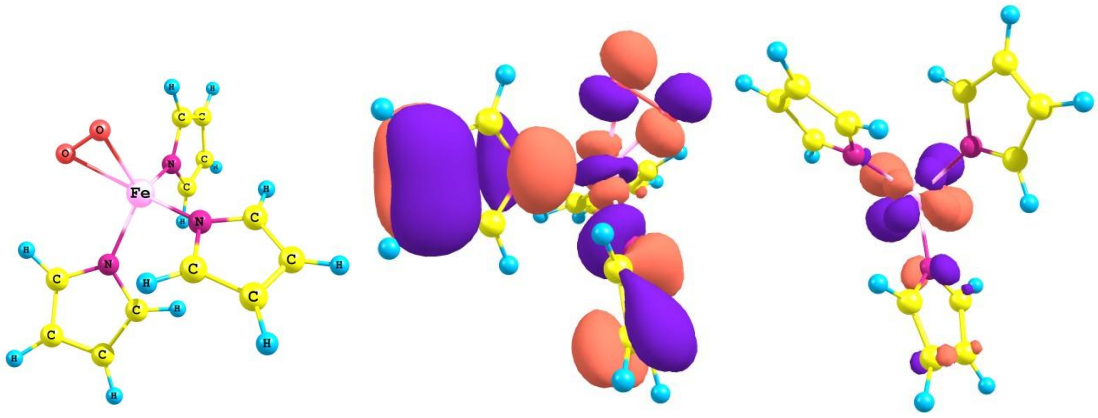

(a) (b) (c)

α HOMO -5 (-7.38 eV) β HOMO -1(-6.06eV)

Fig. 4. Side-on interaction of O_2 with Fe-(3)pyrrole (a), the important MOs; HOMO-5 (b) and HOMO-1 for optimized configuration of O_2/Fe-(4)pyrrole.

Tabel II. Comparison of total valence charge population in O_2 and Fe-(4)pyrrole and for the optimized O_2/Fe-(4)pyrrole system

	Before O_2 adsorption	After O_2 adsorption	Difference
Fe valence orbital population	6.31	6.29	0.02
3Pyrrole valence orbital population	66.87	66.34	0.53
O_2 valence orbital population	11.93	12.48	-0.55

Conclusion

Electronic structure analysis indicates that the elongation of O_2 on Fe–(n)Ppy is induced by the interaction between the Fe d-orbitals and the O_2 anti-bonding orbital. The large elongation of the O_2 bond when adsorbed on Fe–(n)Ppy is due to the formation of a side-on configuration especially for Fe–(4)Ppy with 13.3% elongation as compared with the Fe–(6)Ppy cluster. This will ease O_2 dissociation and enhance the ORR mechanism

Reference

[1] R. Bahsyam and P. Zelenay: Nature 443 (2006) 63

[2] H.K. Dipojono et al : J. Phys. Soc. Jpn., Vol. 78 (2009), No.9

[3] M. J. Frisch et al.: Gaussian 03, Revision D.02 (Gaussian, Inc., Wallingford, CT, 2004)

[4] European commission. A Hydrogen Energy and Fuel Cells, A Vision of Our Future. EUR 20719 EN (2003)

[5] Hydrogen Fuel Cell, Scientific blogging, Agustus 16, 2010.
http://www.science20.com/news_articles/hydrogen_fuel_cells_no_catalyst_needed

[6] Wang, B Recent development of non-platinum catalyst for oxygen reduction reaction. J Power Sources 152, 1-15 (2005)

[7] C. Medard, M Lefevre, J.P. Dodelet, F Jaouen, G. Lindbergh: Electrohimica Acta 51 (2006) 3202-3213

[8] R, Bahsyam and P. Zelenay: Nature 443 (2006) 63.

[9] P. J. Stephens, F. J. Devlin, C. F. Chabalowski, and M. J. Frisch:J. Phys. Chem. 98 (1994) 11623; A. D. Becke: Phys. Rev. A 38 (1988) 3098; C. Lee, W. Yang, and R. G. Parr: Phys. Rev. B 37 (1988) 785.

[10] E. D. Glendening, A. E. Reed, J. E. Carpenter, and F. Weinhold. Theoretical Chemistry Institute and Department of Chemistry, University of Wisconsin, Madison, Wisconsin 53706

Life as a Short Term Student in Osaka University

By: Hani Fadinna

To know that I accepted as QEDC short term students made me not only happy but very happy. To be here, at Japan it just like my dreams becoming true. Honestly at the first three month I was confused what should I do?, everybody has busy with his own project and I think I am nothing and not enough smart to be here and wasn't good compared to another. It's Ok!! Those of bad feeling were fading away. People just need sometimes to know their surrounding right?

I have been living in JASSO dormitory for almost eleventh month until now. There, I could knowing each other from different country, different culture, different language and different life style, but we realized we are united, were living in Japan, we appreciate those of Japanese culture which anything well arranged and everybody well behave.

The most grateful is I'm being a part of Kasai Laboratory Member. At the first sight I was proud to be here, I met Kasai Sensei, and I felt that sensei to much kind like my Lecturer in Indonesia Prof. Hermawan. Every student in Laboratory has a schedule of face to face meeting with Kasai Sensei in every week. Until now I'm about feeling guilty to sensei because sometime I didn't stick to my work, he is too kind and humble. I would like to thank to Kasai Sensei for giving me an opportunity to be a part of Kasai Laboratory Member. Otsukaresama sitsurei shimasu

Although I have finished all of my credit semester for finishing my bachelor degree in my home university ITB-Indonesia, here in Osaka University I took some undergraduate class. The class I attended are presented in Nihongo which sometimes it feel so hard to understand but as I explain above, Japanese always trying to give their best to another, again I'm so grateful I met another kindly person Lecturer namely Goto Sensei. He always translated for every single word he wrote on green board in English and explains with very patient.

I have been doing my research for Fe-polypryrrole, which in fact I have been started since my last semester in ITB and today I still got tide up to report it into the paper worked. I have difficulties to arrange word by word. I realized I need to much learn, effort and consistence to be able to write. Japan is well known for its advance in science, technology, and industry while maintaining high belief in traditional cultures. With this his condition, soon I believe, is become high motivation for another future students in pursuing QEDC program in Osaka University, one of the most pride university in Japan.

It's not that much hard to well adapted in Osaka. I met so many Indonesian and moreover they are my senior in the same major from ITB. Here I feel so amazed to see so fast rescue and work of secretary in Kasai Laboratory. Thanks To Tanaka-san who always taking me care for a bunch of administration problem that I can't handled it only by me and also all of member and staff of Kasai Laboratory.

I'm enjoying every single time in Japan. I have a look so many events, I can attend to international class seminar, I can even join to CMD workshop in Kyoto with free of accommodation. I finally accustomed to present my research and to be brave to talk with the stranger.

I don't know how many word to describe my grateful and, I feel these so wonderful, happy and overwhelming has got experience to live abroad. These preliminary experiences were brought me in highly regarded country Japan and escaped in friendly Suita-shi Osaka-fu. Someday I believe I will miss this place missing the discipline people, full of smile and fast paced in action.

Osaka, August 16, 2010

Knight Shift of Hydrogen in NiTi

from First-Principles Theory : Korringa-Kohn-Rostoker Method

Irma Syafitri[1], Masako Ogura[2], Hisazumi Akai[2]

[1]Engineering Physics, Bandung Institute of Technology, Indonesia

[2]Department of Physics, Osaka University, Japan

Abstract

NiTi alloys near stoichiometry show structural transformation from the monoclinic B19' martensitic phase into cubic B2 austenitic phase by increasing temperature. Many investigations have been made on the process of this martensitic transformation using various experimental techniques. In the present study, we theoretically discuss the possibility of the muon spin rotation (μ-SR) experiment to study the martensitic transformation of NiTi. We examine the stable positions of a muon in NiTi by using the first-principles approach, Korringa-Kohn-Rostoker method. The most stable position is found to be the octahedral site where a muon is surrounded by two nickel and four titanium atoms for both the cubic and monoclinic phases. We also calculate the Knight shift at the muon sites. The obtained values show that the μ-SR experiment can be a reasonable tool to investigate the martensitic transformation of NiTi.

Keyword : Knight shift, NiTi, Hydrogen, Korringa-Kohn-Rostoker method

I. INTRODUCTION

Nitinol or nickel titanium is a kind of material that can be transformed from the monoclinic B19' martensitic phase into the cubic B2 austenitic phase. The transformation is most commonly used as applications of SMAs (shape-memory alloys) such as eyeglass frames, antenna element wire for portable cellular telephones, mixing valves or automatic oil valve adjusting device for shinkansen (the bullet train). There are basically three ways [1] to achieve the sequential B2 – R – B19' transformation in NiTi: by cold work, aging of the alloys with higher Ni content, or addition of third element e.g. Fe and Cu, [2].

Many investigations have been made on transformation process using various experimental techniques [1-10]. The in-situ experimental techniques combined with neutron and ultrasonic wave speed measurement determined that the deformation/transformation processes related to the R-phase affect the thermomechanical responses of NiTi wire and bar specimens [3]. Another interesting experimental technique is positron lifetime measurement in NiTi alloys. The pre-martensitic phenomenon in NiTi was found by an anomalous positron lifetime change above martensitic transformation temperature for $Ni_{51}Ti_{49}$[4], B2-NiTi [5] and NiTiCu [2]. In

addition, anomalous phenomena such as negative temperature coefficient of electrical resistivity [6], decreasing of sound velocity [7], increasing internal friction [8], softening of elastic shear constant [9], and X-ray diffraction patterns [10] have been observed. These phenomena have attracted much attention in the relation to the precursor of the martensitic transformation [4].

The muon spin rotation (μ-SR) is one of powerful methods to experimentally obtain the local information of the electronic structure and magnetism of solids. NiTi shows a large change in the magnetic susceptibility at the martensitic transformation. In the μ-SR measurement, it is expected that a similar change would be observed in the muon Knight shift. The Knight shift is a shift in nuclear magnetic resonance frequencies due to the spin polarization of the conduction electrons at the nuclear site caused by the external magnetic field. In other wards, the shift occurs as a result of paramagnetic effects of the conduction electrons in the vicinity of the nuclei and is proportional to the hyperfine field produced by electron magnetization at the nuclear (muon) position [12]. The muon Knight shift is expected to show behaviors associated with the pre-martensitic phenomenon like the positron lifetime measurement.

In order to discuss the μ-SR experiments, we first of all have to know the location of the muon. However, it is difficult to determine the position only from the experiments.

In this paper, the possible locations of a muon in NiTi and the Knight shift of muon are investigated for both the cubic B2 and monoclinic B19' phases. Applying the Born–Oppenheimer approximation, we simulate a muon in NiTi as a $+e$ charged impurity. We calculate the electronic structure of NiTi with muon impurities from the first-principles and the position of a muon and the Knight shift at the muon site is determined. From the obtained results, we discuss the possibility of the μ-SR experiment to study the martensitic transformation of NiTi.

II. COMPUTATIONAL DETAILS

The total energy and knight shift are computed by using MACHIKANEYAMA computer code [14] that is based on KKR (Korringa-Kohn-Rostoker) method in the framework of the local density approximation (LDA) of the density functional theory. For LDA exchange correlation potentials, the parameterization by Morruzi, Janak and Williams [15] is used.

In this investigation, we use two kinds of structure of NiTi, cubic B2 phase (Fig.1) and monoclinic B19' phase (Fig.2). The cubic B2 austenite is in Pm3m and its lattice constant is a = 3.0125 Å at 300 K. The monoclinic B19' martensite is in $B2_1/m$ and has a = 2.8815 Å, b = 4.1232 Å, c = 4.6256 Å, and $\beta = 97^0$ at 202 K. These

lattice parameters are determined by the neutron diffraction [3]. In this calculation, we use supercells of $(NiTi)_8$ as are shown in Fig.1 and 2.

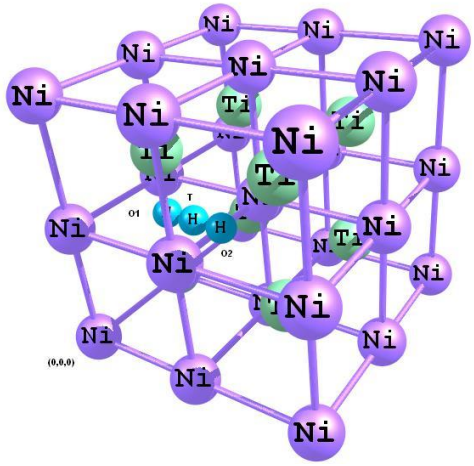

Figure 1. Supercell for the cubic B2 austenitic structure of NiTi. Three kinds of muon (H) sites are also indicated.

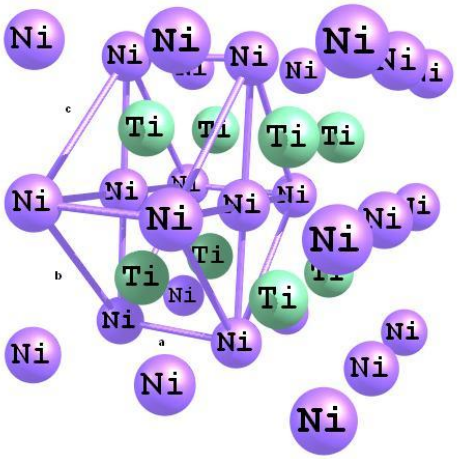

Figure 2. Supercell for the monoclinic B19' martensitic structure.

A muon is supposed to occupy the tetrahedral or octahedral interstitial site in the supercell. In the cubic B2 phase, two kinds of octahedral site can be defined: In the octahedral site 1 (O1 site), the muon is located at the

octahedron that consists of two titanium and four nickel atoms. On the other hand, in the octahedral site 2 (O2 site), the muon is surrounded by two nickel and four titanium atoms. In the tetrahedral site (T site), the muon is in the tetrahedron formed by two titanium and two nickel atoms (see Fig. 3 and 4).

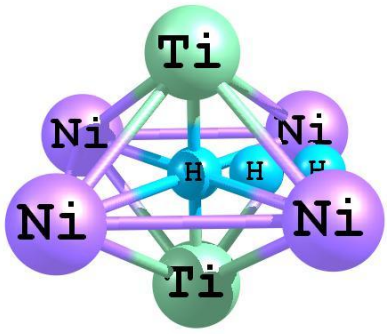

Figure 3. Position of a muon (H). Octahedral site 1 (O1 site, left blue sphere), octahedral site 2 (O2 site, middle blue sphere), and tetrahedral site (T site, right blue sphere).

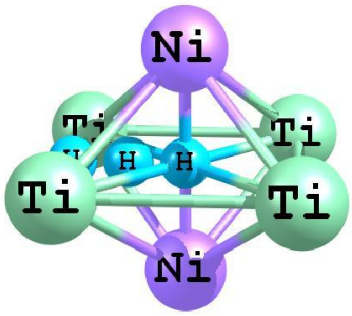

Figure 4. Position of a muon (H). O1 site (left blue sphere), O2 site (middle blue sphere), and T site (right blue sphere).

For the monoclinic B19' phase, we define the supercell composed of a triclinic Bravais lattice in order to compare the calculation in the cubic and monoclinic phases directly. We obtain $a = 2.8815$Å, $b = c = 3.0983$ Å, $\alpha = 83.426^0$ and $\beta = \gamma = 84.78^0$ using the data of monoclinic B19' [3].

In order to estimate the position of the muons in the cubic NiTi, the total energy was examined moving the muon from the O1 to O2 sites through the T sites. In these procedures, the muffin-tin radii of the nickel, titanium and muon atoms are fixed.

Hyperfine field is calculated for the octahedral and tetrahedral sites. Since the hyperfine field is sensitive to the number of *k*-points used for the *k* integral over the Brillouin zone, we check the convergence about the number of *k*-points. The Knight shift *K* can be obtained from the hyperfine field H_{hf},

$$K = \frac{H_{\mathrm{hf}}}{H_{\mathrm{ext}}},$$

where H_{ext} is the external magnetic field.

III. RESULT AND DISCUSSION

First, we discuss the stable position of a muon. Figure 5 shows the calculated total energy in the cubic B2 phase when the position of a muon is changed from the O1 site ($x = 0.25a$) to the O2 site ($x = 0.5a$) through the T site ($x = 0.375a$). In this calculation, $y = 0.25b$ and $z = 0.5c$ are fixed. From Fig. 5, it is clear that the O2 site is the most stable among these positions.

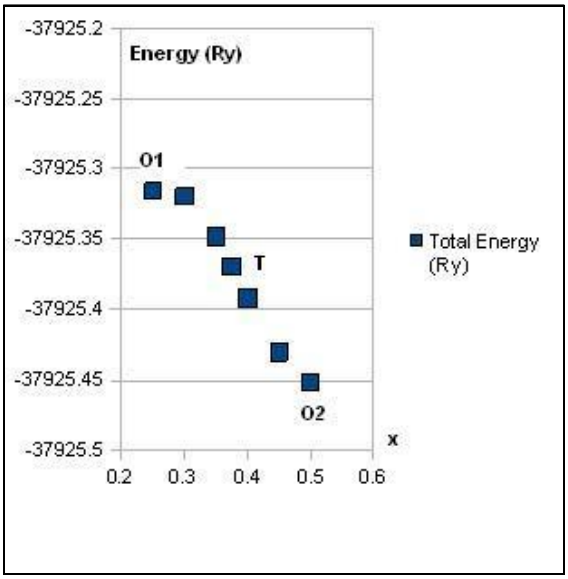

Figure 5. Total energy of NiTi:Mu in the cubic B2 phase.

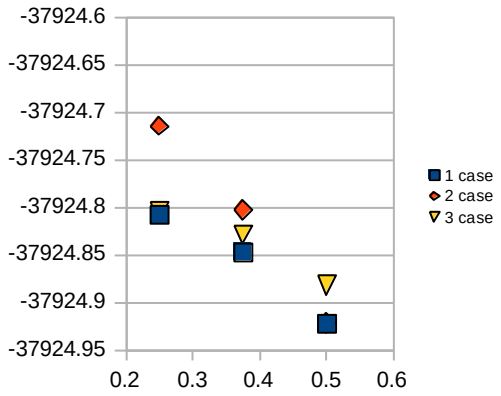

Figure 6. Total energy of NiTi:Mu in the monoclinic B19' phase.

Figure 6 shows the calculated total energy of NiTi:Mu in the monoclinic B19' phase. In this case, we have three kinds of O–T–O paths: In the first case (the blue squares in Fig. 6), the position of a muon is changed from the O1 site (x = 0.25a) to the O2 site (x = 0.5a) through the T1 site (x = 0.375a) and y = 0.25b and z = 0.5c are fixed. In the second case (the orange diamonds in Fig. 6), a muon is moved along the path O3 (y = 0.25b) – T2 (y = 0.375b) – O4(y = 0.5b) with fixed x = 0.5a and z = 0.25c. In the third case (the yellow triangles in Fig. 6), the path is O5 (z = 0.25c) – T3 (z = 0.375c) – O6(z = 0.5c) with fixed x = 0.25a and y = 0.5b. The O1 and O5 sites are equivalent and the O2 and O4 sites are also equivalent. From Fig. 6, we can see that the sites where the muon is surrounded by two nickel and four titanium atoms are stable. Because this tendency is the same in the cubic phase, it is expected that a muon does not change the position before and after the martensitic transformation in NiTi. The O2 site is the most stable because the distance between the muon and nickels is larger in this site than the O6 site.

Figure 7 shows the Knight shift at the muon site in cubic B2 austensitic NiTi. The Knight shift at the O2 site is 3% larger than that at the T site and 25% larger than that at the O1 site.

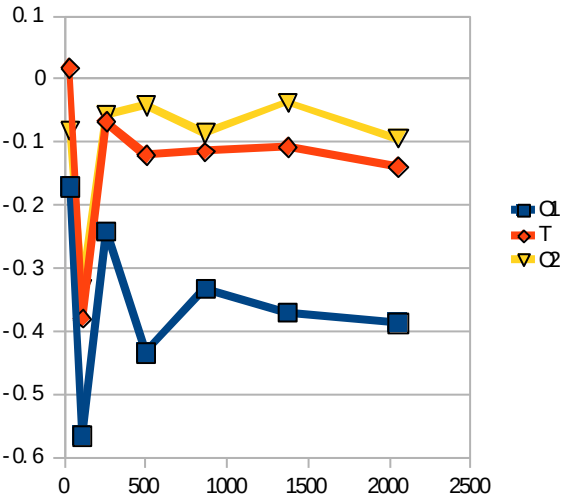

Figure 7. Knight shift at muon site in cubic B2 austensitic NiTi.

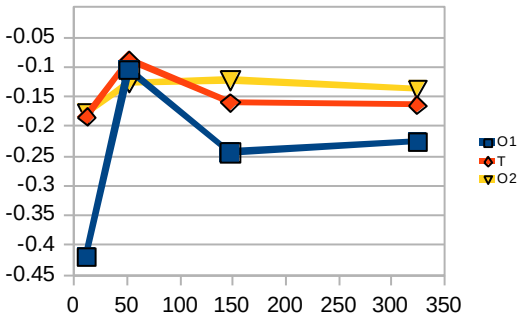

Figure 8. Knight shift at the muon site in monocinic B19' martensitic NiTi.

Figure 9 shows the Knight shift at the muon site in monoclinic B19' martensitic NiTi of the first case. The Knight shift at the O2 site is 6% larger than that at the T site and 9% larger than that at the O1 site. The Knight shift at the O2 site in the monoclinic phase is 40% smaller than that in the cubic phase. This difference is sufficiently large for μ-SR to be used for the investigation of the martensitic transformation of NiTi alloys.

IV. CONCLUSIONS

In the present study, we investigate the stable position and Kight shift of a muon in NiTi in both the cubic B2 austenitic and monoclinic B19' martensitic structures by using the first-principles electronic structure calculation. The octahedral-site-2 where a muon is surrounded by two nickel and four titanium atoms is the most stable position both before and after the martensitic transformation. The Knight shifts at the O1, O2 and T sites are large enough to be detected by the μ-SR experiment. Since the difference in the Knight shift in the cubic and monoclinic phases is also large, the μ-SR experiment is expected to be a powerful method to investigate the martensitic transformation of NiTi alloys.

REFERENCES

[1] Saburi, T., 1998. TiNi—shape memory alloys. In : Otsuka, K., Wayman, C.M. (Eds.), Shape Memory Materials. Cambridge University Press, pp. 49-96.

[2] J. Katsuyama, H. Araki, M. Mizuno, Y. Shirai, Science and Technology of Advance Material. 5 (2004) 41-45.

[3] P. Sittner, M. Landa, P. Lukas, V. Novak, Mechanics of Materials. 38 (2006) 479-45.

[4] H. Araki, N. Matake, P. Chalermkarnnon, Y. Shirai, Mater. Sci. Forum. 327-328 (2000) pp. 437-440.

[5] J. Katsuyama, T. Kobayashi, P. Chalermkarnnon, M. Mizuno, H. Araki, Y. Shirai, Mater. Trans. 43 (2002) 1489-1493.

[6] G.D. Sandrock, Met. Trans., 5 (1974), p. 229.

[7] F.E. Wang, B.F. Deavagge, W.J. Buechler and W.R. Hosler, J. Appl. Phys., 39 (1968), p.2166.

[8] R.R. Hasiguti and K. Iwasaki, J. Appl. Phys., 39 (1968), p. 2182.

[9] O. Mercier, K.N. Melton, G. Gremaud and J. Haegi, J. Appl. Phys., 51 (1980), p. 1833.

[10] G.D. Sandrock, A.J. Perkins and R.. Hehemnn, Met. Trans., 2 (1971), p. 2769.

[11] R.L. Havill, J.M. Titman and N. Cowlam, Hyperfine Interaction. 64 (1990) 665-670.

[12] W.D. Knight, Letter to Editor. (1949) 1259-1260.

[13] Xiangyang Huang, Graeme J. Ackland and Karin M.Rabe, Nature Materials. 2 (2003) 307-311.

[14] H. Akai, M. Ogura, S. Blogel, B. Drittler, H. Ebert, K. Terakura, R. Zeller, and P.H. Dederichs, Progress of Theoretical Physics Supplement, 101 (1990) 11-77.

[15] V. L. Moruzzi, J. F. Janak and A. R. Williams, Calculated Electronic Properties of Metals (Pergamon, U. S. A, 1978).

Life as a short term student in Osaka University

Irma Shafitri

QED-C (Quantum Engineering Design-Course) is one kind of program from Osaka University that offer to foreign student to study in computational research field. As QED-C short term course, I can follow some activities, such as seminar, students meeting, or party. Seminar can give me experience how to convey our research to the others interestingly. In students meeting, I can discuss about our research and how to solve the problem with professor, sensei, and the other student. It's gives so many experience how to do research well. And beside that I can attend many kind of party, such as tea party, BBQ party, mochi party, welcome party etc. We can know japanese culture and each other by this activity. In QED-C program, I also have workshop or seminar at another city like kyoto. From this activity I can know students from the other university.

Japan is country which has 4 seasons. In every season it has special festival called "Matsuri". In autumn, we can see momiji (yellow leaf) from the momiji tree, sakura on spring and hanabi in the summer. The biggest Hanabi (Fireworks) is in the Yokogawa, and I saw it. That is wonderfull hanabi that I ever saw. Actually I only have once see the hanabi.

Finally,I want to say thank you for Tanaka-san and Kasai-sensei who give me information about QED-C program. And I want to say thank you to Akai-sensei, Ogura-sensei, Dino-sensei that give me so many experience how to do research well.

A Theoretical Study on the Effects of Hydrogen Peroxide Adsorption on Pristine and Fe-filled Single-walled Carbon Nanotubes using Density Functional Theory

Joaquin Lorenzo Valmoria Moreno

I. Introduction

Background

Carbon nanotubes (CNTs) filled with magnetic atoms have been receiving a great deal of interest due to their very high potential in providing modified magnetic properties, low dimensionality, and small volume that open possibilities for many applications. Recently, CNT research has focused on device applications such as field effect transistors and fuel cell technology – as catalyst support for oxygen reduction in the cathode of the proton exchange membrane fuel cell (PEMFC) [1-2]. It is necessary to note however, that the role of hydrogen peroxide (H_2O_2) formation is an important part of the characterization of novel fuel cell catalysts [3]. H_2O_2 can appear as an intermediate of by-product in the reaction of hydrogen and oxygen gases to form water. In the presence of trace metals, H_2O_2 decomposes into hydroxyl radicals that can attack and damage the fuel cell membrane and catalyst layers. Furthermore, it has been found that pristine semiconducting single-walled carbon nanotubes (SWNTs) are selectively oxidized when treated with hydrogen peroxide [4].

Fe-filled SWNTs

Our research group has done previous theoretical studies on the effects of Fe in SWNTs. In particular, the diameter dependency of the magnetic and electronic properties of Fe-filled SWNTs has been clarified [5]. Fe-filled SWNTs with diameters of about 4 Å exhibit semiconducting characteristics and no spin polarization, whereas larger diameters exhibit ferromagnetic and metallic characteristics. In addition, Fe-filled SWNTs were found to transform into an arch-like structure when Fe is near a Ni(111) surface [6-9]. In order to determine the feasibility of Fe-filled SWNTs as catalyst material for the PEMFC, studies on adsorption reactions of O, O_2, H_2O, and H_2O_2 are presently being conducted. This paper focuses on the effects of H_2O_2 on Fe-filled SWNTs.

Objectives

The main objective of the study is to investigate the adsorption of H_2O_2 on Fe-filled SWNT. Specifically, the study aims to compare the adsorption of H_2O_2 on Fe-filled SWNT with pristine SWNT. The presence of energy barriers and the most stable structures are investigated as well.

II. Computational Method

Theoretical Model

Reactions of the following systems with H_2O_2 were investigated: (3,3) pristine SWNT, (3,3) Fe-filled SWNT, (5,5) pristine SWNT, and (5,5) Fe-filled SWNT. The supercells were made up of two SWNT unit cells, with the addition of two Fe atoms for the Fe-filled cases. Thus, the (3,3) cases have 24 carbon atoms in the supercell whereas the (5,5) cases have 40 carbon atoms. In the initial calculations, three kinds of adsorption sites for H_2O_2 were taken into account: top (T) site, bridge (B) site, and hollow (H) site. (Fig. 1)

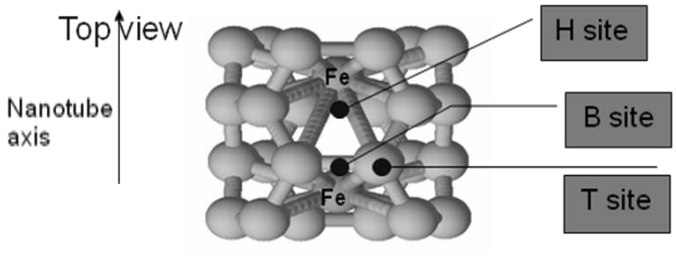

Figure 1. The unit cell of (3,3) Fe-filled SWNT is shown, as well as the three adsorption sites for H_2O_2.

Computational Parameters

The adsorption possibilities for H_2O_2 on the SWNTs were examined by obtaining the total energy of each system as a function of the H_2O_2 molecule's distance from the SWNT surface through static and fully-optimized single-point energy (SPE) calculations. Spin-polarized density functional theory calculations were implemented within the plane wave and pseudopotential method [10]. The Brillouin zone was sampled using 35 k-points along the nanotube axis. Generalized gradient approximation (GGA) was used for the exchange-correlation energy.

III. Results

Molecular Adsorption

The results from the static SPE calculations are shown in Table 1. The minimum energies obtained indicate weak interaction between H_2O_2 and the SWNT. The equilibrium distance was found to be 3.75 Å for most cases. Optimization at the equilibrium distances indicated that the H_2O_2 was molecularly adsorbed on the SWNTs.

Table 1. Equilibrium distances and minimum energies obtained from SPE calculations

	(3,3) SWNT		**(5,5) SWNT***	
	Distance (Å)	**Energy, E_P (meV)**	**Distance (Å)**	**Energy, E_P (meV)**
Pristine B-site	4.00	-17	3.75	-14
Pristine T-site	3.75	-16	3.75	-14
Pristine H-site	3.75	-16	3.75	-16
Fe-filled B-site	3.75	-18	-	-
Fe-filled T-site	3.75	-15	-	-
Fe-filled H-site	3.75	-16	-	-

*Calculations for (5,5) Fe-filled SWNT are still ongoing

Dissociative Chemisorption

Fully-optimized SPE calculations were implemented for (3,3) pristine and Fe-filled SWNT, using the equilibrium distance obtained from the static SPE calculations as the reference point. The results (Table 2) revealed a small energy barrier of about 30-50 meV separating the reference point and the most stable configuration. In addition, the most stable structures indicated dissociative chemisorption, wherein the H_2O_2 has dissociated into hydroxyl radicals and adsorbed on T-sites. Thus, the energy barriers could be attributed to the dissociation of H_2O_2. The optimized structures having the H-site as the reference point

were found to be the most stable for both pristine and Fe-filled cases, and the hydroxyl units were adsorbed onto opposite T-sites. (Fig 2)

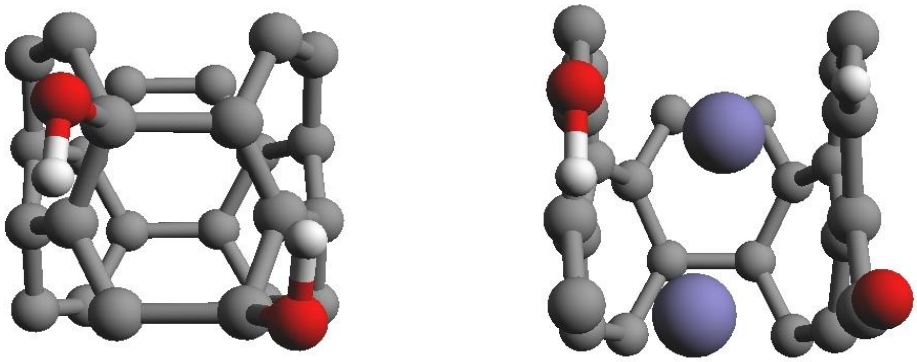

(a) (b)

Figure 2. Stable structures obtained from optimized SPE calculations for (a) (3,3) pristine SWNT and (b) (3,3) Fe-filled SWNT.

Table 2. Lowest energies (E_C) and dissociation energy barriers (E_D) obtained from fully-optimized SPE calculations.

	(3,3) Pristine SWNT		(3,3) Fe-filled SWNT	
	Energy, E_C (eV)	Energy, E_D (meV)	Energy, E_C (eV)	Energy, E_D (meV)
B-site	-2.37	54	-4.62	46
T-site	-2.41	34	-4.64	17
H-site	-2.56	35	-7.76	29

Hydroxyl pair adsorption

Since we know from the results of the (3,3) cases that H_2O_2 dissociates into hydroxyl radicals, the most stable structures for the (5,5) cases can be obtained by optimizing hydroxyl pairs adsorbed on different combinations of T-sites. From the most stable structures (Fig. 3), we can see that the hydroxyl radicals adsorbed on alternating T-sites for pristine SWNT. The circular structure of the SWNT is maintained and

there is no magnetization present. On the other hand, the radicals adsorbed linearly for Fe-filled SWNT. Furthermore, the SWNT structure transformed into a teardrop shape and each of the Fe atoms has a magnetization of 1 μ_B. The adsorption energy is greater for Fe-filled SWNT (-3.36 eV) as compared with pristine SWNT (-1.87 eV).

IV. Summary and Conclusion

The adsorption of H_2O_2 in all cases involves both molecular adsorption and dissociative chemisorption. In the cases of (3,3) pristine and Fe-filled SWNT, an energy barrier was found that could be linked to the dissociation of H_2O_2 into hydroxyl radicals. These radicals were adsorbed in T-sites for all cases. However, bond-breaking of some C-C bonds were observed for the semiconducting (3,3) Fe-filled SWNT. This was not observed in the three metallic cases. This finding supports that the selective oxidation of semiconducting CNTs could also hold true for Fe-filled SWNT and not just for pristine SWNT. Further analysis is needed to confirm this. The presence of energy barriers for the (5,5) cases also needs to be investigated.

References

[1] A. Dicks, J. Power Sources **156** (2006) 108.

[2] E. Lafuenta, et al. J. Mater. Res. **21** (2006) 2841.

[3] V. Sethuraman, et al. Electrochimica Acta **54** (2009) 5571.

[4] Y. Miyata, et al. J. Phys. Chem. B. **110** (2006) 128.

[5] M. Kisaku, et al. Jpn. J. Appl. Phys. **44** (2005) 882.

[6] M. David, et al. Jpn. J. Appl. Phys. **45** (2006) 2869.

[7] M. David, et al. J. Magn. Magn. Mater. **310** (2007) e748.

[8] M. David, et al. Surf. Sci. **601** (2007) 4366.

[9] M. David, et al. e-J. Surf. Sci. Nanotechnol. **3** (2005) 256.

[10]B. Hammer, et al. Phys. Rev. B **59** (1999) 7413.

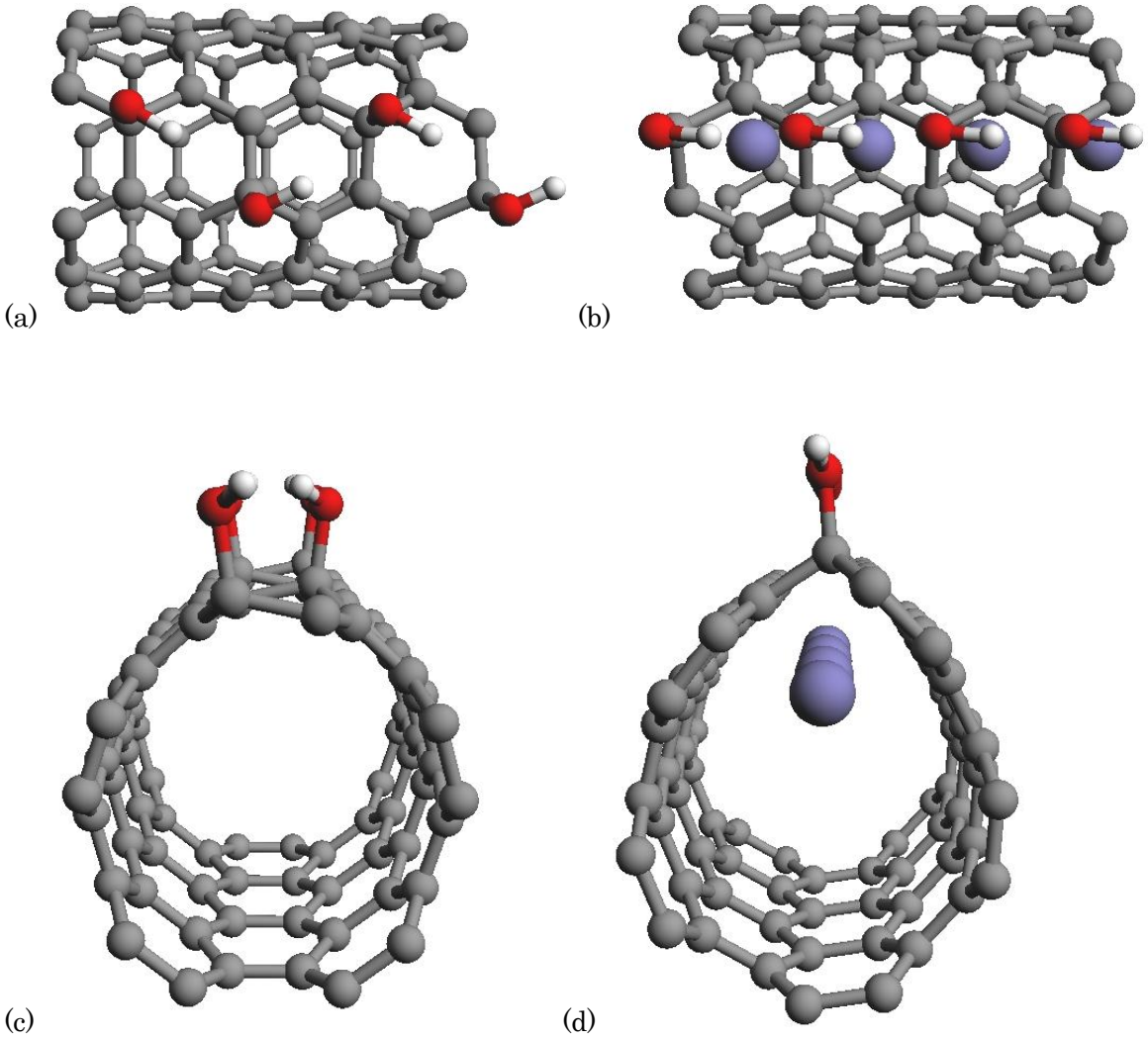

Figure 3. Most stable structures for adsorption of hydroxyl radicals. Shown are the top view for (a) (5,5) pristine SWNT and (b) (5,5) Fe-filled SWNT, as well as the side view into nanotube axis for (c) (5,5) pristine SWNT and (d) (5,5) Fe-filled SWNT.

Opportunity – My Life as a QEDC Student

Joaquin Lorenzo Valmoria Moreno

If there is one word to summarize my experience as a QEDC student, that word would be “opportunity.”

Before I start talking about my life as an exchange student under the QEDC short term course, let me first mention the motivations why I wanted to become an exchange student. First of all is the opportunity to become a better researcher. Second is the opportunity for cultural exchange. And lastly, there is the opportunity to become a more independent person. These three opportunities were the reasons why I wanted to be a QEDC student.

In the QEDC short term course, academic courses are not required. Thus, I was able to concentrate on conducting research. However, in the laboratory we were not limited to doing just that. I was assigned to do several other tasks such as refereeing journals, giving lectures, and being part of collaboration projects with companies and other universities. But the thing I like the most is attending conferences and meetings. In these events, I am able to present my research to other researchers of my field and get feedback from them. Because of this, I am able to gain new ideas about my research. I also get to interact with the leaders of my field. Aside from this is the opportunity to travel and see new places. During my stay, I attended conferences or workshops in Awaji Island, Kyoto, Takamatsu, and Nagoya.

Ritsurin Garden in Takamatsu, Kagawa Pref. (left) and Nagoya University in Nagoya, Aichi Pref. (right)

Part of being an exchange student is experiencing a culture different from your own. And here in Japan, the first obstacle for foreigners is the language barrier. I took advantage of this opportunity to learn about a new culture. Knowledge of basic Japanese is necessary to enjoy my stay here in Japan to the fullest. And during my stay, I eventually grew fond of the Japanese way of living. I started to enjoy the local dishes, and even the music, movies, anime and TV shows. Immersing myself in all these made it easier for me to adapt. It keeps me from becoming lonely and homesick. I also get to do things that I seldom do, such as hiking and skiing. Finally, it is very important to respect the local beliefs and traditions. Experiencing New Year's Day in the temple and attending the summer matsuri are examples of some traditional events.

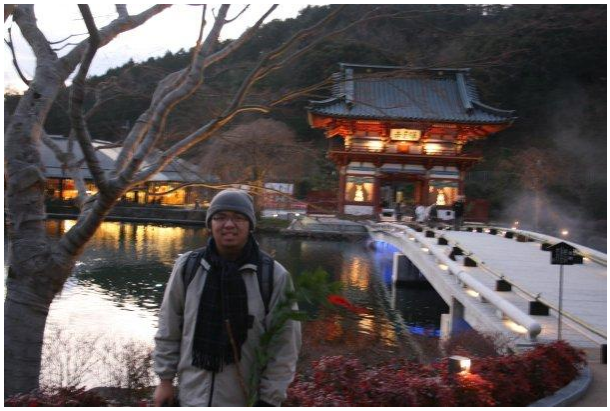

Celebrating New Year's Day at Katsuo-ji (left) and skiing in Myoko, Niigata (right)

One of the most difficult things about being an exchange student is living away from home. This experience has taught me many things about life such as making a budget for your daily expenses and managing your bills among others. Also doing housekeeping chores like cooking, washing the dishes, and doing my laundry are some things I only got to do during my days as an exchange student. These little things, I used to take for granted. But as an exchange student away from home, I learned to do all these things and have now become a more independent person.

Becoming a better researcher, experiencing a different culture, and being more independent – these opportunities that I foresaw in the QEDC short term exchange program have all been fulfilled. And upon completing this course, the possibilities for the future are endless. New opportunities are created.